

A Catalog of Habitable Zone Exoplanets

MICHELLE L. HILL,¹ KIMBERLY BOTT,¹ PAUL A. DALBA,^{2,1,*} TARA FETHEROLF,^{1,†} STEPHEN R. KANE,¹
RAVI KOPPARAPU,^{3,4,5} ZHEXING LI,¹ AND COLBY OSTBERG¹

¹*Department of Earth and Planetary Sciences, University of California Riverside, 900 University Ave, Riverside, CA 92521, USA*

²*Department of Astronomy and Astrophysics, University of California, Santa Cruz, CA 95064, USA*

³*NASA NExSS Virtual Planetary Laboratory, Seattle, WA USA*

⁴*Blue Marble Space Institute of Science, Seattle, WA USA*

⁵*NASA Goddard Space Flight Center, Greenbelt, MD USA*

ABSTRACT

The search for habitable planets has revealed many planets that can vary greatly from an Earth analog environment. These include highly eccentric orbits, giant planets, different bulk densities, relatively active stars, and evolved stars. This work catalogs all planets found to reside in the HZ and provides HZ boundaries, orbit characterization, and the potential for spectroscopic follow-up observations. Demographics of the HZ planets are compared with a full catalog of exoplanets. Extreme planets within the HZ are highlighted, and how their unique properties may affect their potential habitability. Kepler-296 f is the most eccentric $\leq 2 R_{\oplus}$ planet that spends 100% of its orbit in the HZ. HD 106270 b and HD 38529 c are the most massive planets ($\leq 13 M_J$) that orbit within the HZ, and are ideal targets for determining the properties of potential hosts of HZ exomoons. These planets, along with the others highlighted, will serve as special edge-cases to the Earth-based scenario and observations of these targets will help test the resilience of habitability outside the standard model. The most promising observational targets are HD 102365 b and 55 Cnc f, and the best candidates that are $\leq 2 R_{\oplus}$ are GJ 667 C c, Wolf 1061 c, Teegarden’s Star b, and Proxima Cen b.

Keywords: planetary systems – techniques: photometric – techniques: radial velocities

1. INTRODUCTION

Exoplanet discoveries over the past several decades have revealed a vast diversity of planetary architectures (Ford 2014; Winn & Fabrycky 2015), and shown that terrestrial planets are far more common than their giant planet counterparts (Borucki 2016). In these ongoing exoplanet searches, discovering those planets that may harbor life has been a primary objective for the astrobiology community (Fujii et al. 2018; Schwieterman et al. 2018; Glaser et al. 2020; Lisse et al. 2020). A potential pathway toward the identification of such worlds is to constrain the stellar and planetary parameter space that may allow for the presence of surface liquid water. Such is the premise of the habitable zone (HZ), defined as the region around a star where water can exist in a liquid state on the surface of a planet with suffi-

cient atmospheric pressure (Kasting et al. 1993; Kopparapu et al. 2013, 2014; Kane et al. 2016). The HZ broadly consists of two main regions; the conservative habitable zone (CHZ) and the optimistic habitable zone (OHZ), shown in Figure 1 as the light green and dark green regions, respectively. The CHZ inner boundary is the runaway greenhouse limit, during which water loss can occur through photodissociation of water molecules in the upper atmosphere. The CHZ outer boundary is the maximum greenhouse, where the planetary temperature conditions allow condensation of substantial atmospheric CO_2 on the surface (Kopparapu et al. 2013). The OHZ inner boundary, the Recent Venus limit, is based on the empirical observation that the surface of Venus has been dry for at least a billion years, but may have had conditions suitable for surface liquid water prior (Kane et al. 2014; Way et al. 2016). The outer edge of the OHZ, the Early Mars limit, is based on evidence that Mars appears to have harbored surface liquid water ~ 3.8 Gya (Kopparapu et al. 2013).

mhill012@ucr.edu

* NSF Astronomy and Astrophysics Postdoctoral Fellow

† Chancellor’s Postdoctoral Fellow

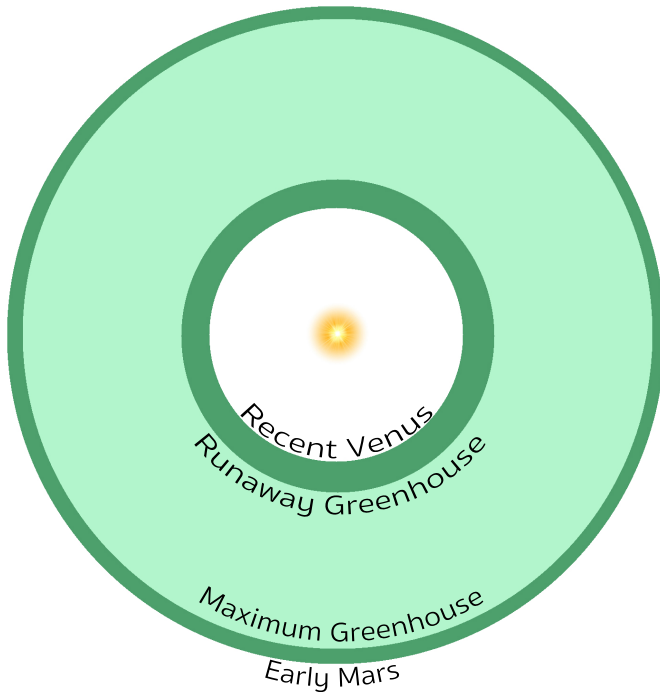


Figure 1. Depiction of both the conservative (light green) and optimistic (combined light and dark green) HZ regions, with boundary labels defined by [Kopparapu et al. \(2013\)](#).

The HZ has undergone numerous revisions to incorporate scenarios quite different to Earth, such as tidal locking ([Yang et al. 2014](#)), desert environments ([Abe et al. 2011](#)), and substantial methane greenhouse warming ([Ramirez & Kaltenegger 2018](#)). Although these revisions often extend the possible surface liquid water environments, it has also been suggested that the HZ may not be restrictive enough for supporting complex life ([Schwieterman et al. 2019](#)). Even so, the HZ has been a critical component of calculating the occurrence rate of terrestrial planets potentially amenable to temperate surface conditions ([Dressing & Charbonneau 2013](#); [Bryson et al. 2021](#)) and the demographics of the HZ planet population ([Adams & Kane 2016](#)). These methodologies have been extended to consider the occurrence of giant planets in the HZ that may harbor temperate moons ([Heller 2012](#); [Hill et al. 2018](#)) and the prevalence of potential Venus analogs ([Kane et al. 2014](#)). Dynamical simulations have been utilized to determine regions of orbital stability within the HZ that could harbor further terrestrial planets ([Kopparapu & Barnes 2010](#); [Kane et al. 2020](#)). Of the thousands of known exoplanets, hundreds reside within the HZ ([Kane & Gelino 2012b](#)), and the extent of the HZ has been calculated for many nearby stars using available stellar data ([Chan-](#)

[dler et al. 2016](#); [Kopparapu et al. 2018](#)). The tracking and cataloging of HZ planets is an important task for the purposes of designing efficient follow-up strategies to further characterize their planetary properties ([Kane et al. 2016](#); [Kopparapu et al. 2018](#)). This need is particularly heightened in the era of the Transiting Exoplanet Survey Satellite (TESS; [Ricker et al. 2015](#)), whose exoplanet discoveries around bright host stars will be particularly amenable to near-term atmospheric characterization ([Kempton et al. 2018](#)). On longer time scales, mission concepts, such as LUVOIR ([The LUVOIR Team 2019](#)), the Habitable Exoplanet Observatory (HabEx; [Gaudi et al. 2020](#)), and the recommendations of the Astro2020 report ([of Sciences Engineering & Medicine 2021a](#)), will provide further opportunities to understand the current state and evolution of habitable surface environments. As thousands of exoplanets have already been discovered, and both current and future exoplanet missions will only increase that number, the HZ is still an essential tool to refine the list of potentially habitable planets for target selection in future observational campaigns.

In this paper, we present a catalog of HZ planets that includes all known exoplanetary systems, irrespective of detection method, for which their properties allow the determination of their HZ status. This catalog updates previous HZ catalogs and extends the catalog to include all HZ planets, not just those from a specific mission (i.e. Kepler ([Gaidos 2013](#); [Hill et al. 2018](#))). The focus of this HZ catalog is the demographics of the known HZ exoplanet population and the prospects for follow-up observations that will best serve the community in the fulfillment of the Astro2020 report recommendations. In Section 2, we describe the data extraction, criteria for inclusion, and the calculations for the catalog assembly. Section 3 presents the main catalog data for the exoplanets that meet our selection criteria, including measured and calculated properties for the stars and planets. In Section 4, we provide a discussion of the catalog demographics, including analysis of outliers and the primary targets for follow-up opportunities. We outline the overall features of the catalog, proposed expansion and exploitation opportunities, and further concluding remarks in Section 5.

2. DATA EXTRACTION AND CALCULATIONS

The full data set of known exoplanets was downloaded from the NASA Exoplanet Archive ([Akeson et al. 2013](#); [NASA Exoplanet Archive 2022](#)) using the Application Programming Interface (API). The default values for each planet were downloaded and are used in the calculations and discussion that follows. More about the

use of only the default values can be found in Section 4. Planets with no stellar effective temperature (T_{eff}) were removed from the list. For planets that were missing stellar luminosity (L_{\odot}), luminosity was calculated using the Stefan-Boltzmann law. When unavailable, the stellar radius (R_{\odot}) was calculated from the stellar mass (M_{\odot}) and surface gravity ($\log g$). Stellar luminosities, and therefore HZ boundaries, can be sensitive to the uncertainties associated with their calculation (Kane 2014; Chandler et al. 2016; Kane 2018). In cases where luminosity was missing and could not be calculated, the planet was removed from the sample. The stellar mass and planet orbital period (P) were used to calculate the semi-major axis (a) of planets if it was missing from the NEA. If the semi-major axis data was missing and it was not able to be calculated, the planet was removed from the sample.

HZ boundaries were calculated via the method described by Kopparapu et al. (2013, 2014). Four HZ boundaries were calculated for each planet and are presented in Table 1: Recent Venus (R1), Runaway Greenhouse (R2), Maximum Greenhouse (R3), and Early Mars (R4). The percentage of time each planet spent in the CHZ and OHZ was calculated by solving Kepler’s equation for each planet’s orbit. Planets were included in the HZ table if they spent any amount of time in the OHZ. We chose to include all planets that spent time in the HZ, no matter how briefly, to account for the uncertainty in HZ boundaries and orbital parameters.

Table 1 includes a column that indicates how much of a planet’s orbit is spent within the CHZ and OHZ. The list also includes planets of all sizes, regardless of whether they are expected to be in the terrestrial or gaseous regime. This is to include any planets that may be host to terrestrial exomoons, which are also potentially habitable worlds.

Only 15 planets on the list had both a mass and radius measurement, the remaining planets having only one or the other measured, and so the mass-radius relationship from Chen & Kipping (2017) was used to determine these values for planets that were missing either mass or radius information. We used the probabilistic modeling tool `forecaster` to estimate planet mass or radius based on the mass-radius relation from Chen & Kipping (2017) that spans from dwarf planets to late-type stars. We chose to use the Chen & Kipping (2017) relation for consistency across our sample of planets, although we note that there are other mass-radius relations that may be well suited to specific planet regimes (such as Thorngren et al. (2019) for cool giant planets, and Wolfgang et al. (2016); Weiss & Marcy (2014) for planets $< 4 R_{\oplus}$). We recommend further investigation

into these other mass-radius relations for any individual planets the reader is interested in that is missing mass or radius measurement information, particularly for the planets with measured radii $> 9 R_{\oplus}$ for which mass measurements were estimated, as there is a large degeneracy in the mass estimations from Chen & Kipping (2017) in this region. The mass and radius values that were calculated using the mass-radius relationship are included in Table 1 and are distinguished by *italic font* and are missing uncertainty values.

Planet equilibrium temperature (T_{eq}) was calculated from luminosity (assuming an albedo of 0) and subsequently used to calculate the transmission spectroscopy metric (TSM) value of each planet (Kempton et al. 2018). The TSM is proportional to the expected transmission spectroscopy signal-to-noise, based on the strength of spectral features, brightness of the host star, and mass and radius of the planet assuming cloud-free atmospheres. The method for calculating the TSM is only applicable for planets $< 10 R_{\oplus}$, therefore TSM is not included for planets with larger radii in Table 1.

To account for any planets whose eccentricity values were set to zero as a default value, rather than measured, eccentricity values were filtered for the histogram and scatter plots to only include planets with eccentricity uncertainty measurements. Additionally, the planets that have eccentricity fixed to zero are listed as 0 in Table 1, whereas eccentricities that were measured as 0 are listed as 0.00. Note that those eccentricities that are fixed to zero means that they may be considered lower limits on those values.

3. CATALOG OF HZ EXOPLANETS

Here we present the catalog of HZ exoplanets. Each planet listed in these tables passes through the OHZ at some point in their orbit. No cutoff has been made for the amount of time the planet must spend in the HZ. As planets that orbit outside the HZ temporarily are expected to be able to maintain or regain habitable periods (Williams & Pollard 2002; Kane & Gelino 2012a; Way & Georgakarakos 2017; Palubski et al. 2020; Kane et al. 2021), planets that spend any time in the HZ (from here referred to as $> 0\% \text{HZ}$) are included in the catalog.

Table 1 includes the planet parameters for the HZ planets, and Table 2 includes the stellar parameters. The two tables are available combined as one master table in machine-readable format and can be filtered by the “% in HZ” columns as needed. Table 1 is ordered by the % time the planet spends in the CHZ followed by time in the OHZ then followed by the planet name. Table 2 is ordered by star name.

Planet mass (M_P) and radius (R_P) are included in Table 1. Measured values of each include uncertainty values in the table. Mass and radius values that have been calculated using the mass-radius relationship from [Chen & Kipping \(2017\)](#) are distinguished with both *italic font* and are missing uncertainty values.

Columns R1, R2, R3, and R4 list the Recent Venus, Runaway Greenhouse, Maximum Greenhouse, and Early Mars HZ boundaries respectively. Planetary orbital period (P), semi-major axis (a), incident flux (flux) and eccentricity (e) are also included in the Table 1.

Planets whose TSM values are missing lack T_{eq} information, or the means to calculate it, or their parameter values were outside the limits set in the paper (i.e. $\geq 10 R_{\oplus}$).

Within Tables 1 and 2 and denoted by an exclamation point (!) next to the planet name are six planets that are marked as controversial in the NEA at the time of printing. These are HD 40307 g, KIC 5951458 b, GJ 667 C e, GJ 667 C f, Kepler-452 b, and Kepler-186 f ([Díaz et al. 2016a](#); [Dalba et al. 2020](#); [Robertson & Mahadevan 2014](#); [Mullally et al. 2018](#); [Burke et al. 2019](#)). As these planets are still listed as confirmed in the NEA we have elected to retain these planets in our sample. However, we recommend further investigation into their validity if any of these planets are of interest for follow-up. Further discussion as to why these planets are listed as controversial is included in Section 4.4.

There are five circumbinary planets (CBPs) that have orbits that spend time the HZ. These are listed sepa-

rately in Table 3. The table includes planet mass (M_p), radius (R_p), orbital period (P), semi-major axis (a), eccentricity (e), stellar mass of primary ($M_{*,A}$), stellar radius of primary ($R_{*,A}$), effective temperature of primary ($T_{eff,A}$), $\log g$ of primary, luminosity of primary ($L_{*,A}$), J magnitude (J), stellar mass of secondary ($M_{*,B}$), stellar radius of secondary ($R_{*,B}$). Further discussion of these systems is in Section 4.3.

Figures 2 and 3 show distributions of planet and stellar parameters for the entire exoplanet catalog (gray), the $> 0\%$ HZ planets (light green), planets that spend 100% of the time in the OHZ (100%HZ; medium green), and planets $< 2 R_{\oplus}$ that spend 100% of the time in the OHZ (Rocky-OHZ; dark green). As of printing 4586 planets had sufficient data to be included in the full catalog, 328 planets in the $> 0\%$ HZ subset, 143 planets in the 100%HZ subset, and 29 planets in the Rocky-OHZ subset. In order to directly compare the groups, the bin sizes are the same for each group. Sturges' rule was applied to the full catalog group to determine the appropriate histogram bin sizes and then used for all groups.

Scatter plots including measured values of mass and radius alongside those with [Chen & Kipping \(2017\)](#) values can be found in Figure 4. Each of these is color coded with a third parameter: TSM, J or density.

Figures 5 and 6 include scatter plots of the entire exoplanet catalog (gray) versus the $> 0\%$ HZ planets (green). These plots also include a heat map to allow easy identification of clusters and their relative density.

Table 1. Habitable Zone Planet Properties.

Name	M_p [†]	R_p [†]	P	a	e	Flux	R1	R2	R3	R4	CHZ	OHZ	TSM	K
	M_{\oplus}	R_{\oplus}	days	AU		W/m^2	AU	AU	AU	AU	%	%		m/s
GJ 3293 d	$7.6^{+1.05}_{-1.05}$	<i>2.67</i>	48.13	0.194	0.12	797.6	0.121	0.154	0.299	0.315	100	100	145.1	2.4
GJ 357 d	6.1^{+1}_{-1}	<i>2.33</i>	55.66	0.204	0	522.3	0.103	0.131	0.254	0.268	100	100	168.6	2.1
GJ 667 C c	$3.81^{+1.5}_{-1.2}$	<i>1.73</i>	28.14	0.125	0.02	1197.6	0.096	0.122	0.238	0.251	100	100	150.7	1.7
GJ 667 C e (!)	$2.54^{+1.6}_{-1.4}$	<i>1.31</i>	62.24	0.213	0.02	412.5	0.096	0.122	0.238	0.251	100	100	11.4	0.9
GJ 667 C f (!)	$2.54^{+1.4}_{-1.2}$	<i>1.33</i>	39.03	0.156	0.03	768.9	0.096	0.122	0.238	0.251	100	100	13.9	1.0
GJ 682 b	$4.4^{+3.7}_{-2.4}$	<i>1.89</i>	17.48	0.080	0.08	426.5	0.037	0.047	0.093	0.098	100	100	–	2.6
HD 10442 b	$472.61^{+24.16}_{-24.16}$	<i>13.46</i>	1032.30	2.010	0.132	685.4	1.120	1.419	2.577	2.718	100	100	–	29.9
HD 106270 b	$3219.62^{+85.81}_{-85.81}$	<i>12.3</i>	1888.00	3.340	0.185	716.0	1.844	2.336	4.152	4.379	100	100	–	135.5
HD 10697 b	$2028.71^{+24.79}_{-24.79}$	<i>12.56</i>	1075.69	2.140	0.104	843.3	1.276	1.616	2.864	3.021	100	100	–	116.9
HD 111998 b	$1433.41^{+158.92}_{-158.92}$	<i>12.84</i>	825.90	1.820	0.03	1438.0	1.338	1.694	2.942	3.103	100	100	–	87.3
HD 114729 b	$262.21^{+2.22}_{-2.22}$	<i>13.83</i>	1121.79	2.067	0.079	723.0	1.124	1.424	2.507	2.645	100	100	–	16.9
HD 159868 b	$704.95^{+18.75}_{-18.75}$	<i>13.07</i>	1184.10	2.320	0.024	968.9	1.488	1.885	3.347	3.531	100	100	–	37.9
HD 1605 c	$1150.54^{+73.1}_{-73.1}$	<i>12.9</i>	2149.00	3.584	0.099	686.1	1.998	2.531	4.596	4.848	100	100	–	47.3
HD 163607 c	$699.54^{+11.76}_{-11.76}$	<i>13.14</i>	1272.00	2.390	0.08	618.0	1.225	1.552	2.757	2.908	100	100	–	38.4

Table 1 continued

Table 1 (continued)

Name	M_p \dagger	R_p \dagger	P	a	e	Flux	R1	R2	R3	R4	CHZ	OHZ	TSM	K
	M_\oplus	R_\oplus	days	AU		W/m^2	AU	AU	AU	AU	%	%		m/s
HD 165155 b	$918.53^{+73.1}_{-73.1}$	13.05	434.50	1.130	0.2	748.1	0.641	0.812	1.446	1.526	100	100	–	78.0
HD 17674 b	$276.51^{+22.25}_{-19.07}$	13.75	623.80	1.420	0.13	1028.3	0.918	1.163	2.044	2.156	100	100	–	21.1
HD 18015 b	$1010.7^{+73.1}_{-73.1}$	13.06	2278.00	3.870	0.148	790.1	2.233	2.828	5.012	5.286	100	100	–	38.0
HD 188015 b	$476.75^{+41.32}_{-41.32}$	13.36	461.20	1.203	0.137	977.5	0.765	0.970	1.711	1.805	100	100	–	37.6
HD 216435 b	$400.47^{+41.3}_{-41.3}$	13.53	1311.00	2.560	0.07	610.3	1.267	1.605	2.816	2.970	100	100	–	19.7
HD 221585 b	$511.71^{+44.5}_{-44.5}$	13.36	1173.00	2.306	0.123	678.3	1.231	1.560	2.763	2.914	100	100	–	27.8
HD 23079 b	$829.54^{+34.96}_{-34.96}$	13.02	730.60	1.600	0.1	698.1	0.849	1.075	1.886	1.989	100	100	–	54.8
HD 28185 b	$1875.2^{+76.28}_{-76.28}$	12.65	379.00	1.020	0.05	1284.4	0.748	0.947	1.675	1.767	100	100	–	163.1
HD 34445 f	$37.82^{+6.5}_{-6.5}$	6.72	676.80	1.543	0.031	1151.9	1.060	1.343	2.364	2.494	100	100	108.9	2.6
HD 45364 c	209.1	13.89	342.85	0.897	0.097	966.9	0.578	0.732	1.305	1.376	100	100	–	21.9
HD 564 b	$104.88^{+9.54}_{-9.54}$	12.82	492.30	1.200	0.096	1053.5	0.785	0.995	1.748	1.844	100	100	–	8.8
HD 73534 b	$353.43^{+18.75}_{-18.75}$	13.72	1750.00	2.990	0.126	533.4	1.470	1.862	3.380	3.565	100	100	–	17.1
HD 9174 b	$352.79^{+44.5}_{-44.5}$	13.55	1179.00	2.200	0.12	679.7	1.179	1.493	2.648	2.793	100	100	–	21.1
HD 99109 b	$139.85^{+25.43}_{-25.43}$	14.01	439.30	1.110	0.09	743.6	0.633	0.801	1.435	1.513	100	100	–	14.2
K2-288 B b	4.55	$1.87^{+0.3}_{-0.3}$	31.39	0.164	0	596.3	0.089	0.112	0.220	0.232	100	100	–	1.9
KELT-6 c	$1179.15^{+66.74}_{-66.74}$	12.87	1276.00	2.390	0.21	777.2	1.313	1.664	2.901	3.060	100	100	–	65.4
Kepler-1086 c	8.65	$2.87^{+0.11}_{-0.13}$	161.52	0.515	0	719.8	0.301	0.381	0.709	0.748	100	100	5.0	1.3
Kepler-1143 c	11.81	$3.52^{+0.51}_{-0.35}$	210.63	0.646	0	1135.9	0.460	0.583	1.053	1.110	100	100	5.5	1.5
Kepler-1229 b	2.82	$1.37^{+0.11}_{-0.13}$	86.83	0.312	0	669.3	0.178	0.226	0.432	0.456	100	100	0.5	0.6
Kepler-1318 b	9.02	$3.04^{+0.17}_{-0.15}$	213.26	0.629	0	678.5	0.353	0.448	0.824	0.869	100	100	5.3	1.2
Kepler-150 f	11.56	$3.57^{+0.52}_{-0.39}$	637.21	1.240	0	612.8	0.633	0.801	1.424	1.501	100	100	3.4	0.9
Kepler-1540 b	6.21	$2.44^{+0.19}_{-0.14}$	125.41	0.444	0	1260.3	0.340	0.431	0.796	0.839	100	100	8.4	1.0
Kepler-1544 b	4.1	$1.74^{+0.09}_{-0.07}$	168.81	0.557	0	1231.9	0.417	0.528	0.960	1.012	100	100	3.7	0.5
Kepler-1600 b	9.11	$3.06^{+0.28}_{-0.17}$	386.37	0.987	0	624.9	0.518	0.656	1.177	1.241	100	100	2.6	0.9
Kepler-1628 b	34.71	$6.3^{+0.94}_{-0.51}$	76.38	0.289	0	765.0	0.176	0.223	0.429	0.452	100	100	15.6	7.8
Kepler-1634 b	9.02	$3.13^{+0.52}_{-0.6}$	374.88	0.990	0	890.1	0.610	0.773	1.376	1.451	100	100	4.4	0.8
Kepler-1635 b	12.56	$3.57^{+0.33}_{-0.67}$	469.63	1.137	0	559.5	0.560	0.710	1.268	1.337	100	100	2.7	1.1
Kepler-1636 b	9.8	$3.16^{+0.76}_{-0.35}$	425.48	1.111	0	1167.1	0.770	0.975	1.719	1.813	100	100	1.8	0.8
Kepler-1649 c	2.02	$1.04^{+0.15}_{-0.1}$	19.54	0.083	0	1022.9	0.059	0.075	0.147	0.155	100	100	1.0	1.4
Kepler-1652 b	3	$1.57^{+0.18}_{-0.18}$	38.10	0.165	0	1148.3	0.124	0.157	0.303	0.319	100	100	6.1	1.1
Kepler-174 d	5.2	$2.14^{+0.13}_{-0.13}$	247.35	0.677	0	582.9	0.348	0.441	0.803	0.847	100	100	5.4	
Kepler-186 f (!)	2.2	$1.14^{+0.08}_{-0.08}$	129.94	0.432	0.04	402.0	0.191	0.242	0.464	0.489	100	100	0.4	0.4
Kepler-1868 b	9.59	3.08 \pm	211.03	0.627	0	697.7	0.357	0.452	0.829	0.875	100	100	9.8	1.3
Kepler-283 c	4.1	$1.78^{+0.12}_{-0.12}$	92.74	0.341	0	1227.3	0.260	0.329	0.613	0.646	100	100	3.3	
Kepler-442 b	2.88	$1.32^{+0.11}_{-0.18}$	112.31	0.409	0.04	954.3	0.274	0.348	0.646	0.681	100	100	0.3	0.5
Kepler-454 c	$1417.52^{+38.14}_{-38.14}$	12.77	523.90	1.284	0.021	898.5	0.786	0.995	1.759	1.855	100	100	–	110.0
Kepler-553 c	2267.97	$10.96^{+0.32}_{-0.31}$	328.24	0.906	0	830.1	0.546	0.691	1.239	1.306	100	100	–	221.2
Kepler-62 f	2.65	$1.38^{+0.07}_{-0.07}$	267.29	0.718	0	555.8	0.360	0.456	0.828	0.873	100	100	0.3	0.3
Kepler-68 d	$244.73^{+9.53}_{-9.53}$	13.84	634.60	1.474	0.112	1070.1	0.973	1.233	2.169	2.288	100	100	–	17.6
Kepler-705 b	4.84	$2.06^{+0.1}_{-0.08}$	56.06	0.232	0	1136.9	0.173	0.219	0.420	0.443	100	100	6.8	1.2
Kepler-712 c	19.42	$4.75^{+0.26}_{-0.41}$	226.89	0.687	0	1109.9	0.482	0.610	1.098	1.158	100	100	5.1	2.3
Kepler-97 c	≥ 343.26	13.57	789.00	1.637	0	490.0	0.736	0.932	1.644	1.734	100	100	–	24.7
KIC 10525077 b	26.51	$5.39^{+0.9}_{-0.8}$	854.08	1.768	0	550.8	0.827	1.047	1.833	1.933	100	100	3.1	1.8
KIC 5951458 b (!)	35.44	$6.46^{+26.3}_{-4.2}$	1320.10	2.339	0	793.7	1.300	1.647	2.873	3.030	100	100	6.1	2.1
KIC 9663113 b	17.87	$4.5^{+0.6}_{-0.7}$	572.38	1.340	0	979.7	0.837	1.060	1.857	1.959	100	100	5.5	1.4
LHS 1140 b	$6.38^{+0.46}_{-0.44}$	$1.6^{+0.05}_{-0.05}$	24.74	0.096	0.096	484.5	0.047	0.059	0.118	0.125	100	100	83.4	4.3
Teegarden's Star c	$1.11^{+0.16}_{-0.15}$	1.05	11.41	0.044	0.00	507.4	0.022	0.028	0.056	0.059	100	100	105.3	1.6
TOI-1227 b	1086	$9.37^{+0.75}_{-0.58}$	27.36	0.089	0	436.8	0.041	0.052	0.103	0.109	100	100	3.4	741.5
TRAPPIST-1 e	$0.69^{+0.02}_{-0.02}$	$0.9^{+0.013}_{-0.012}$	6.10	0.029	0	882.9	0.019	0.025	0.050	0.053	100	100	26.3	1.2
TRAPPIST-1 f	$1.04^{+0.03}_{-0.03}$	$1.02^{+0.013}_{-0.012}$	9.21	0.038	0	509.9	0.019	0.025	0.050	0.053	100	100	22.3	1.6
TRAPPIST-1 g	$1.32^{+0.04}_{-0.04}$	$1.11^{+0.02}_{-0.01}$	12.35	0.047	0	344.4	0.019	0.025	0.050	0.053	100	100	20.3	1.8

Table 1 continued

Table 1 (continued)

Name	M_p $^{\pm}$	R_p $^{\pm}$	P	a	e	Flux	R1	R2	R3	R4	CHZ	OHZ	TSM	K
	M_{\oplus}	R_{\oplus}	days	AU		W/m^2	AU	AU	AU	AU	%	%		m/s
HD 63765 b	$168.45^{+9.53}_{-9.53}$	14.02	358.00	0.940	0.24	842.4	0.565	0.716	1.274	1.344	98	100	–	20.8
HD 27969 b	$1525.58^{+76.28}_{-73.1}$	12.71	654.50	1.552	0.182	1039.7	1.005	1.273	2.234	2.357	96	100	–	103.2
HD 181720 b	$127.13^{+19.07}_{-19.07}$	14	956.00	1.850	0.26	872.2	1.113	1.409	2.488	2.624	91	100	–	8.4
BD-06 1339 c	54.03^{+8}_{-8}	8.53	125.94	0.435	0.31	685.8	0.248	0.314	0.586	0.618	90	100	471.3	9.2
GJ 180 c	$6.4^{+3.7}_{-4.1}$	2.37	24.33	0.129	0.09	1066.5	0.093	0.118	0.231	0.244	89	100	–	2.5
HD 10180 g	$23.27^{+4.39}_{-4.39}$	5.19	604.67	1.427	0.263	905.3	0.865	1.096	1.926	2.031	89	100	112.3	1.8
HD 147513 b	384.57^{+}	13.54	528.40	1.320	0.26	765.6	0.737	0.934	1.642	1.732	86	100	–	29.4
WASP-47 c	$398.2^{+9.3}_{-9.3}$	13.36	588.50	1.393	0.296	779.9	0.801	1.014	1.800	1.899	84	100	–	31.0
GJ 1148 b	$96.7^{+1.41}_{-1.02}$	12.3	41.38	0.166	0.38	669.8	0.095	0.121	0.237	0.250	84	100	–	39.7
BD+14 4559 b	$330.54^{+149.38}_{-149.38}$	13.62	268.94	0.780	0.29	833.9	0.481	0.609	1.108	1.168	84	100	–	55.0
HIP 56640 b	$1166.44^{+60.39}_{-60.39}$	12.93	2574.90	3.730	0.12	1100.8	2.651	3.358	6.135	6.471	84	100	–	53.3
HD 40307 g (!)	$7.09^{+2.6}_{-2.6}$	2.53	197.80	0.600	0.29	870.6	0.376	0.476	0.864	0.911	82	100	116.7	1.0
WASP-41 c	$1010.7^{+63.57}_{-63.57}$	13.03	421.00	1.070	0.294	766.0	0.610	0.772	1.371	1.446	81	100	–	94.5
HD 137388 b	$63.57^{+6.36}_{-6.36}$	9.45	330.00	0.890	0.36	863.3	0.549	0.696	1.251	1.319	80	100	248.0	8.2
HD 13908 c	$1630.47^{+79.45}_{-79.45}$	12.88	931.00	2.030	0.12	1324.8	1.458	1.847	3.222	3.398	80	100	–	90.5
TOI-2257 b	4.94	$2.15^{+0.11}_{-0.11}$	35.19	0.145	0.496	775.4	0.089	0.113	0.221	0.233	79	88	34.3	2.3
HD 109286 b	$950.31^{+47.67}_{-47.67}$	13.11	520.10	1.259	0.338	965.6	0.799	1.012	1.788	1.886	79	100	–	81.2
HD 4732 c	$753.26^{+120.77}_{-120.77}$	13.03	2732.00	4.600	0.23	999.1	3.089	3.912	7.091	7.480	78	100	–	24.5
GJ 1061 d	$1.64^{+0.24}_{-0.23}$	1.13	13.03	0.054	0.53	795.0	0.034	0.043	0.086	0.090	78	87	70.3	2.2
Kepler-296 f	3.77	$1.77^{+0.31}_{-0.3}$	63.34	0.255	0.33	849.6	0.164	0.208	0.399	0.420	78	100	5.9	1.0
HD 218566 b	$63.57^{+19.07}_{-19.07}$	9.25	225.70	0.690	0.3	931.0	0.452	0.572	1.047	1.105	77	100	306.6	8.4
HD 108874 b	$451.32^{+28.6}_{-28.6}$	13.53	394.48	1.040	0.13	1228.6	0.748	0.948	1.680	1.772	77	100	–	37.2
HD 183263 b	$1255.43^{+69.92}_{-69.92}$	12.95	626.52	1.490	0.36	1045.4	0.969	1.227	2.154	2.272	77	95	–	83.8
HD 210277 b	$410^{+15.89}_{-15.89}$	13.54	442.19	1.130	0.48	1033.6	0.748	0.948	1.683	1.776	76	86	–	38.9
Proxima Cen b	$1.27^{+0.19}_{-0.17}$	1.09	11.19	0.049	0.35	898.8	0.032	0.041	0.081	0.086	75	94	195.6	1.6
HD 221287 b	$982.09^{+251.08}_{-251.08}$	13.08	456.10	1.250	0.08	1449.9	0.936	1.186	2.067	2.181	74	100	–	70.4
HD 100777 b	$327.36^{+12.71}_{-12.71}$	13.68	383.70	1.030	0.36	1171.1	0.726	0.920	1.634	1.723	71	87	–	34.9
Kepler-443 b	5.71	$2.3^{+0.19}_{-0.22}$	177.67	0.495	0.11	1207.6	0.369	0.468	0.856	0.903	70	100	2.7	0.8
HD 214823 b	$6451.95^{+826.36}_{-826.36}$	12.01	1854.40	3.230	0.164	612.0	1.608	2.037	3.577	3.773	69	100	–	281.6
55 Cnc f	$47.77^{+2.4}_{-2.4}$	7.86	259.88	0.771	0.08	1304.2	0.585	0.741	1.332	1.405	69	100	573.9	5.1
HD 213240 b	$1773.49^{+98.53}_{-98.53}$	12.74	882.70	1.890	0.42	999.7	1.199	1.519	2.665	2.811	68	90	–	96.2
HD 142415 b	$530.78^{+38.14}_{-38.14}$	13.25	386.30	1.060	0.5	1468.7	0.817	1.035	1.818	1.917	68	80	–	51.4
HD 44219 b	$184.34^{+19.07}_{-12.71}$	14.07	472.30	1.190	0.61	1754.1	1.014	1.284	2.266	2.390	65	77	–	19.1
HD 180617 b	$12.21^{+1.05}_{-1.05}$	3.52	105.91	0.343	0.101	375.5	0.147	0.186	0.361	0.381	65	100	431.3	2.7
HD 103891 b	$457.68^{+19.07}_{-15.89}$	13.44	1919.00	3.270	0.31	779.9	1.822	2.308	4.041	4.263	64	91	–	21.0
TOI-700 d	2.11	$1.12^{+0.06}_{-0.06}$	37.42	0.163	0.111	1186.2	0.125	0.158	0.307	0.324	63	100	2.5	0.7
HD 34445 b	$260.62^{+28.6}_{-28.6}$	13.85	1049.00	2.070	0.27	650.7	1.066	1.350	2.375	2.505	61	73	–	15.6
HD 65216 b	$411.59^{+19.71}_{-19.71}$	13.65	577.60	1.301	0.27	621.1	0.665	0.842	1.493	1.574	61	73	–	36.0
PH2 b	1768.24	$9.91^{+0.56}_{-0.56}$	282.53	0.828	0.41	1574.3	0.673	0.853	1.510	1.593	61	77	0.9	196.2
HD 4203 b	$708.76^{+66.74}_{-66.74}$	13.17	431.88	1.170	0.52	1770.3	1.011	1.280	2.269	2.394	61	75	–	60.4
GJ 96 b	$19.66^{+2.42}_{-2.3}$	4.6	73.94	0.291	0.44	1430.1	0.243	0.307	0.588	0.621	60	76	–	4.7
HD 48265 b	$484.69^{+15.57}_{-15.89}$	13.39	778.51	1.814	0.211	1452.5	1.408	1.783	3.149	3.321	59	100	–	28.8
HD 133131 A b	$451.32^{+12.71}_{-12.71}$	13.46	649.00	1.440	0.33	708.2	0.777	0.985	1.736	1.831	57	75	–	36.5
HD 153950 b	$937.6^{+92.17}_{-92.17}$	13.06	499.40	1.280	0.34	1723.8	1.057	1.339	2.342	2.470	57	77	–	69.1
HD 7199 b	$85.81^{+9.53}_{-9.53}$	11	615.00	1.360	0.19	518.8	0.644	0.816	1.457	1.537	57	69	–	7.8
HD 187085 b	$265.71^{+3.5}_{-3.5}$	13.7	1019.74	2.100	0.251	627.6	1.047	1.326	2.319	2.446	56	67	–	15.5
HD 82943 b	$534.27^{+8.9}_{-8.9}$	13.49	441.47	1.183	0.162	1524.5	0.929	1.177	2.068	2.181	56	100	–	43.2
HD 132406 b	$1709.93^{+416.36}_{-416.36}$	12.74	974.00	1.980	0.34	627.8	1.007	1.276	2.250	2.373	53	61	–	114.6
GJ 832 c	$5.4^{+0.95}_{-0.95}$	2.15	35.68	0.163	0.18	1335.9	0.132	0.167	0.325	0.343	51	100	312.6	1.8
HD 92788 b	$1195.04^{+50.85}_{-47.67}$	12.79	325.80	0.970	0.35	1842.8	0.848	1.073	1.895	1.999	51	72	–	107.8
HD 96167 b	$227.88^{+12.71}_{-12.71}$	13.78	498.04	1.332	0.685	2808.4	1.438	1.821	3.215	3.391	51	68	–	21.5

Table 1 continued

Table 1 (continued)

Name	M_p $^{\pm}$	R_p $^{\pm}$	P	a	e	Flux	R1	R2	R3	R4	CHZ	OHZ	TSM	K
	M_{\oplus}	R_{\oplus}	days	AU		W/m^2	AU	AU	AU	AU	%	%		m/s
HD 38529 c	4128.61 $^{+47.67}_{-47.67}$	12.15	2136.10	3.640	0.341	571.4	1.792	2.270	4.031	4.251	50	57	–	172.4
HIP 67537 b	3527.91 $^{+127.13}_{-349.61}$	12.35	2556.50	4.910	0.59	2344.1	5.043	6.388	11.568	12.201	49	68	–	113.3
HD 24040 c	63.88 $^{+8.58}_{-8.58}$	9.27	515.40	1.300	0.11	1560.1	1.043	1.321	2.330	2.458	49	100	167.9	4.8
HD 95089 c	1096.51 $^{+44.5}_{-44.5}$	12.96	1785.00	3.330	0.284	1668.5	2.895	3.667	6.658	7.022	47	74	–	45.1
K2-18 b	8.92 $^{+1.7}_{-1.6}$	2.32 $^{+0.22}_{-0.22}$	32.94	0.143	0.2	1440.9	0.120	0.152	0.296	0.312	46	83	33.0	3.6
HD 137496 c	2434.58 $^{+34.96}_{-34.96}$	12.45	479.90	1.216	0.477	2368.5	1.201	1.521	2.681	2.828	45	66	–	219.4
HD 331093 b	476.75 $^{+34.96}_{-34.96}$	13.39	621.62	1.440	0.59	993.5	0.935	1.184	2.102	2.217	45	65	–	43.3
BD+45 564 b	432.25 $^{+38.14}_{-38.14}$	13.4	307.88	0.830	0.12	1490.5	0.679	0.860	1.557	1.642	44	100	–	47.4
HD 125612 b	985.27 $^{+127.13}_{-127.13}$	13.1	557.04	1.372	0.455	832.6	0.801	1.015	1.786	1.884	44	65	–	80.1
Kepler-1708 b	≤ 1482.35	9.75 $^{+0.6}_{-0.59}$	737.11	1.640	0.4	771.7	0.904	1.145	2.002	2.112	44	67	0.3	107.8
47 UMa b	804.11 $^{+22.25}_{-19.07}$	13.13	1078.00	2.100	0.032	488.3	0.937	1.187	2.088	2.203	43	100	–	48.2
HD 219415 b	317.83 $^{+}$	13.49	2093.30	3.200	0.4	555.7	1.612	2.042	3.723	3.927	43	59	–	17.3
HD 190647 b	630.89 $^{+10.49}_{-10.49}$	13.08	1176.45	2.231	0.224	479.9	1.000	1.267	2.241	2.364	43	52	–	37.4
Ross 508 b	4 $^{+0.53}_{-0.55}$	1.78	10.77	0.054	0.33	1701.5	0.049	0.062	0.124	0.130	43	69	251.7	3.9
HD 148164 b	390.93 $^{+79.46}_{-79.46}$	13.69	328.55	0.993	0.587	2959.7	1.081	1.369	2.399	2.530	42	64	–	39.4
HD 16175 b	1620.93 $^{+257.44}_{-257.44}$	12.61	990.00	2.120	0.6	1032.3	1.367	1.731	3.037	3.204	41	58	–	93.7
HD 94834 b	400.47 $^{+54.03}_{-54.03}$	13.32	1576.00	2.740	0.14	1526.1	2.290	2.901	5.293	5.583	40	100	–	20.7
HD 141937 b	3079.77 $^{+127.13}_{-127.13}$	12.49	653.22	1.500	0.41	686.1	0.794	1.005	1.769	1.865	40	60	–	233.6
HD 45364 b	59.5 $^{+}$	8.85	226.93	0.681	0.168	1676.7	0.578	0.732	1.305	1.376	40	88	265.0	7.2
Kepler-440 b	4.23	1.87 $^{+0.24}_{-0.19}$	101.11	0.242	0.34	1843.0	0.227	0.288	0.542	0.572	40	66	6.7	0.9
HD 23596 b	2870 $^{+235.19}_{-235.19}$	12.4	1561.00	2.770	0.27	497.6	1.235	1.565	2.742	2.892	40	47	–	126.6
HD 197037 b	251.09 $^{+16}_{-16}$	13.72	1035.70	2.070	0.22	495.0	0.915	1.158	2.025	2.136	40	48	–	15.2
BD-00 4475 b	7961.64 $^{+708.76}_{-708.76}$	11.81	723.20	1.480	0.39	450.2	0.664	0.842	1.521	1.604	40	45	–	695.3
HD 196050 b	1010.7 $^{+95.35}_{-95.35}$	13.03	1378.00	2.510	0.23	468.6	1.097	1.389	2.444	2.578	39	46	–	49.8
HD 23127 b	485.33 $^{+11.76}_{-12.08}$	13.43	1211.17	2.370	0.406	564.6	1.139	1.443	2.541	2.680	38	48	–	28.0
HD 224538 b	1897.45 $^{+133.49}_{-133.49}$	12.66	1189.10	2.280	0.464	775.0	1.264	1.602	2.803	2.956	37	56	–	106.1
HD 43197 b	190.7 $^{+38.14}_{-12.71}$	13.94	327.80	0.920	0.83	1176.4	0.651	0.825	1.466	1.546	37	52	–	32.6
HD 216437 b	706.54 $^{+18.43}_{-18.43}$	13.26	1334.28	2.497	0.317	463.0	1.083	1.371	2.410	2.542	36	42	–	38.9
HIP 67851 c	1900.62 $^{+241.55}_{-241.55}$	12.62	2131.80	3.820	0.17	1640.7	3.297	4.176	7.592	8.007	36	83	–	69.0
HD 125390 b	7043.11 $^{+305.12}_{-305.12}$	12.02	1756.20	3.160	0.591	2842.8	3.597	4.556	8.295	8.749	36	61	–	373.1
HD 169830 c	1284.03 $^{+}$	12.84	2102.00	3.600	0.33	483.7	1.558	1.973	3.440	3.629	35	40	–	54.2
HD 10647 b	298.76 $^{+25.43}_{-25.43}$	13.82	989.20	2.015	0.15	473.8	0.867	1.099	1.918	2.023	35	46	–	18.1
HD 147379 b	28.55 $^{+1.49}_{-1.45}$	5.78	86.78	0.323	0.07	1398.7	0.264	0.335	0.629	0.664	35	100	–	5.8
HD 132563 b	473.57 $^{+28.6}_{-28.6}$	13.44	1544.00	2.620	0.22	470.5	1.119	1.417	2.471	2.607	35	42	–	23.4
GJ 514 b	5.2 $^{+0.9}_{-0.9}$	2.16	140.43	0.422	0.45	329.2	0.169	0.214	0.411	0.434	34	38	130.9	1.1
Kepler-1654 b	151.41	8.99 $^{+0.213}_{-0.191}$	1047.84	2.026	0.26	409.1	0.841	1.066	1.889	1.992	34	40	2.9	9.8
HD 217786 b	4131.79 $^{+254.25}_{-254.25}$	12.26	1319.00	2.380	0.4	455.0	1.019	1.291	2.267	2.391	33	38	–	257.3
Kepler-296 e	3.07	1.49 $^{+0.27}_{-0.25}$	34.14	0.169	0.33	1934.4	0.164	0.208	0.399	0.420	33	63	0.8	1.0
HD 192310 c	24.16 $^{+5}_{-5}$	5.3	525.80	1.180	0.32	377.0	0.482	0.610	1.097	1.157	33	38	290.8	2.3
HD 120084 b	1430.24 $^{+}$	12.81	2082.00	4.300	0.66	3222.6	5.201	6.588	11.974	12.630	33	60	–	53.3
HD 128356 b	282.87 $^{+22.25}_{-22.25}$	13.61	298.20	0.870	0.57	648.8	0.473	0.599	1.089	1.148	32	45	–	43.9
HD 222582 b	2660.24 $^{+127.13}_{-127.13}$	12.54	572.38	1.340	0.73	979.5	0.851	1.078	1.901	2.005	31	44	–	276.7
HD 170469 b	209.77 $^{+34.96}_{-34.96}$	13.97	1145.00	2.240	0.11	437.5	0.948	1.201	2.114	2.230	30	45	–	12.1
HD 175167 b	2850.94 $^{+1055.2}_{-1055.2}$	12.52	1290.00	2.400	0.54	657.0	1.260	1.596	2.826	2.981	29	42	–	160.6
GJ 273 b	2.89 $^{+0.27}_{-0.26}$	1.44	18.65	0.091	0.1	1445.8	0.077	0.097	0.190	0.200	29	100	67.7	1.6
HD 126614 b	130.31 $^{+19.07}_{-19.07}$	13.45	1244.00	2.370	0.41	365.4	0.932	1.180	2.094	2.208	28	32	–	7.3
HD 196885 A b	820 $^{+50.85}_{-50.85}$	13.12	1333.00	2.370	0.48	583.0	1.129	1.430	2.495	2.632	28	42	–	46.0
HD 156411 b	235.19 $^{+15.89}_{-12.71}$	13.88	842.20	1.880	0.22	2078.9	1.728	2.189	3.849	4.059	28	69	–	14.1
HD 12661 b	772.33 $^{+44.5}_{-44.5}$	13.1	262.71	0.840	0.38	2539.8	0.867	1.098	1.943	2.050	27	59	–	73.7
Kepler-61 b	5.15	2.11 $^{+0.13}_{-0.13}$	59.88	0.258	0.25	1841.1	0.243	0.308	0.583	0.615	27	65	3.9	1.2
GJ 1061 c	1.74 $^{+0.23}_{-0.23}$	1.15	6.69	0.035	0.29	1892.4	0.034	0.043	0.086	0.090	27	63	87.1	2.5

Table 1 continued

Table 1 (continued)

Name	M_p $^{\pm}$	R_p $^{\pm}$	P	a	e	Flux	R1	R2	R3	R4	CHZ	OHZ	TSM	K
	M_{\oplus}	R_{\oplus}	days	AU		W/m^2	AU	AU	AU	AU	%	%		m/s
HD 156846 b	$3391.25^{+235.19}_{-235.19}$	12.32	359.51	1.120	0.85	4851.6	1.555	1.969	3.447	3.636	27	59	–	464.8
HIP 109384 b	$495.81^{+25.43}_{-25.43}$	13.42	499.48	1.134	0.549	544.4	0.556	0.704	1.266	1.335	27	38	–	56.4
HD 4113 b	$495.81^{+12.71}_{-12.71}$	13.55	526.62	1.280	0.903	1015.6	0.833	1.055	1.865	1.967	27	36	–	91.9
HD 191806 b	$2707.91^{+200.23}_{-200.23}$	12.39	1606.30	2.800	0.259	388.0	1.105	1.399	2.453	2.588	27	32	–	139.6
HD 238914 b	$1906.98^{+858.14}_{-858.14}$	12.68	4100.00	5.700	0.56	2974.4	6.659	8.435	15.411	16.255	27	57	–	70.9
BD+49 828 b	$508.53^{+127.1}_{-63.6}$	13.41	2590.00	4.200	0.35	2283.7	4.267	5.404	9.802	10.339	26	60	–	19.1
HD 215497 c	104.88^{+}	12.96	567.94	1.282	0.49	323.1	0.486	0.615	1.109	1.170	26	29	–	10.2
HD 85390 b	$31.47^{+3.18}_{-3.18}$	6.15	799.52	1.373	0.5	380.7	0.563	0.713	1.281	1.351	25	33	118.8	3.0
BD-11 4672 c	$15.37^{+2.97}_{-2.81}$	4.05	74.20	0.300	0.4	2381.8	0.316	0.401	0.739	0.780	25	58	162.2	3.4
HD 141399 d	$375.04^{+25.43}_{-25.43}$	13.61	1069.80	2.090	0.074	424.2	0.884	1.119	1.984	2.092	24	48	–	22.5
HD 11506 b	$1535.12^{+165.27}_{-165.27}$	12.74	1622.10	2.900	0.374	347.0	1.081	1.369	2.399	2.530	24	27	–	77.9
Kepler-1704 b	$1318.99^{+92.17}_{-92.17}$	$11.69^{+0.48}_{-0.46}$	988.88	2.026	0.921	941.6	1.265	1.603	2.829	2.984	24	32	–	199.9
HD 50554 b	$1574.53^{+123.63}_{-123.63}$	12.63	1293.00	2.353	0.501	342.7	0.874	1.107	1.941	2.048	23	26	–	103.7
HD 86264 b	$2224.81^{+508.53}_{-508.53}$	12.56	1475.00	2.860	0.7	762.8	1.563	1.980	3.457	3.646	23	32	–	138.1
HD 20782 b	$472.87^{+33.22}_{-33.88}$	13.47	597.06	1.365	0.95	937.4	0.849	1.075	1.895	1.999	23	31	–	111.9
HAT-P-44 c	$1271.32^{+444.9}_{-254.3}$	12.88	872.20	1.752	0.494	284.5	0.617	0.782	1.399	1.476	22	24	–	101.7
HIP 97233 b	$6356.6^{+127.1}_{-127.1}$	12.08	1058.80	2.550	0.61	3357.9	3.130	3.964	7.168	7.561	22	56	–	322.6
HD 148156 b	$270.16^{+212.94}_{-15.89}$	13.73	1027.00	2.450	0.52	404.4	0.969	1.227	2.139	2.256	22	28	–	17.5
HD 70573 b	1938.76^{+130}_{-130}	12.59	851.80	1.760	0.4	301.6	0.622	0.788	1.392	1.468	21	24	–	142.2
HIP 14810 d	$187.52^{+31.78}_{-31.78}$	14.07	981.80	1.940	0.185	354.4	0.752	0.953	1.691	1.784	21	30	–	12.2
16 Cyg B b	$565.74^{+25.43}_{-25.43}$	13.33	798.50	1.660	0.68	620.8	0.842	1.066	1.881	1.984	21	29	–	50.5
HD 203473 b	$2479.07^{+349.61}_{-349.61}$	12.37	1552.90	2.730	0.289	325.7	1.001	1.267	2.235	2.357	21	26	–	132.0
HD 81040 b	$2310.62^{+311.47}_{-311.47}$	12.78	1001.70	1.940	0.53	295.8	0.679	0.860	1.517	1.600	21	23	–	167.8
HD 8535 b	$216.12^{+22.25}_{-12.71}$	14.02	1313.00	2.450	0.15	409.9	0.986	1.249	2.183	2.303	21	32	–	11.8
HD 13167 b	$1052.02^{+50.85}_{-50.85}$	13.03	2613.00	4.100	0.563	430.7	1.739	2.203	3.897	4.110	20	32	–	48.3
HD 30562 b	$387.75^{+44.5}_{-44.5}$	13.47	1157.00	2.340	0.76	694.5	1.245	1.577	2.773	2.925	20	28	–	33.7
K2-72 e	2.42	$1.26^{+0.14}_{-0.13}$	24.16	0.106	0.11	1514.8	0.091	0.116	0.227	0.239	20	100	2.7	1.3
HD 28254 b	$368.68^{+31.78}_{-19.07}$	13.36	1116.00	2.150	0.81	646.1	1.118	1.416	2.504	2.641	19	25	–	37.3
HIP 57274 d	167.4^{+8}_{-8}	14.01	431.70	1.010	0.27	2072.5	0.990	1.254	2.304	2.431	19	61	–	18.1
HD 106252 b	$2202.56^{+85.81}_{-85.81}$	12.47	1531.00	2.610	0.48	259.2	0.849	1.075	1.891	1.994	18	20	–	137.8
HD 156279 b	$3140.16^{+219.3}_{-219.3}$	12.33	131.05	0.490	0.71	4073.2	0.647	0.820	1.460	1.540	17	55	–	577.1
HD 20868 b	$397.29^{+187.52}_{-187.52}$	13.61	380.85	0.950	0.75	417.1	0.415	0.526	0.959	1.012	16	22	–	99.1
iot Dra c	$4958.15^{+4449.6}_{-1620.92}$	12.11	25000.00	19.400	0.455	191.2	5.806	7.354	13.597	14.341	16	18	–	90.7
HD 45350 b	$568.92^{+44.49}_{-44.49}$	13.28	963.60	1.920	0.778	512.3	0.894	1.132	2.009	2.119	16	22	–	59.4
HD 168443 c	$5464.45^{+66.74}_{-66.74}$	12.16	1749.83	2.837	0.211	315.6	1.041	1.319	2.345	2.474	15	24	–	295.4
HIP 5158 b	451.32^{+}	13.45	345.72	0.890	0.52	189.4	0.260	0.329	0.597	0.630	15	17	–	56.7
HD 8673 b	$4513.19^{+508.51}_{-508.51}$	12.22	1634.00	3.020	0.723	507.1	1.331	1.686	2.935	3.095	15	21	–	298.8
HD 2039 b	$1999.15^{+368.68}_{-368.68}$	12.5	1120.00	2.200	0.71	447.9	0.936	1.186	2.082	2.197	15	21	–	151.8
Kepler-539 c	$762.79^{+381.4}_{-381.4}$	13.04	1000.00	2.420	0.5	216.7	0.722	0.914	1.610	1.699	15	17	–	54.4
HIP 109600 b	$851.78^{+38.14}_{-38.14}$	12.97	232.08	0.706	0.163	1943.4	0.641	0.813	1.443	1.522	14	74	–	98.4
HD 216520 c	$9.44^{+1.63}_{-1.63}$	2.9	154.43	0.528	0.12	1729.3	0.463	0.587	1.057	1.115	14	100	154.6	1.3
HD 39091 b	$3184.66^{+47.67}_{-47.67}$	12.47	2093.07	3.100	0.637	205.3	0.888	1.125	1.971	2.079	14	15	–	193.9
Kepler-419 c	$2320.16^{+127.1}_{-127.1}$	12.49	675.47	1.680	0.184	2247.3	1.555	1.970	3.426	3.614	13	69	–	137.7
BD-17 63 b	$1620.93^{+38.14}_{-38.14}$	12.86	655.60	1.340	0.54	159.6	0.363	0.460	0.843	0.889	13	15	–	172.5
HD 55696 b	$1230^{+228.84}_{-228.84}$	12.79	1827.00	3.180	0.705	363.3	1.214	1.537	2.696	2.843	13	18	–	76.4
HD 114613 b	$113.47^{+10.17}_{-10.17}$	12.99	4000.00	5.340	0.458	199.3	1.544	1.955	3.462	3.651	12	15	–	4.4
HD 131664 b	$6076.91^{+540.31}_{-540.31}$	11.86	1951.00	3.170	0.64	171.4	0.837	1.061	1.865	1.967	12	13	–	356.8
TOI-2285 b	3.66	$1.7^{+0.08}_{-0.08}$	27.27	0.136	0.3	2109.4	0.139	0.176	0.341	0.360	12	58	24.3	1.4
HD 79498 b	$425.89^{+66.74}_{-66.74}$	13.61	1807.00	2.980	0.575	164.7	0.778	0.986	1.740	1.835	11	13	–	25.9
HD 196067 b	$2193.03^{+1239.5}_{-349.6}$	12.59	3638.00	5.020	0.66	202.2	1.429	1.810	3.173	3.347	11	15	–	102.1
HD 211810 b	$212.95^{+139.85}_{-139.85}$	14.08	1558.00	2.656	0.68	227.3	0.820	1.038	1.837	1.938	11	17	–	15.7

Table 1 continued

Table 1 (continued)

Name	M_p $^{\pm}$	R_p $^{\pm}$	P	a	e	Flux	R1	R2	R3	R4	CHZ	OHZ	TSM	K
	M_{\oplus}	R_{\oplus}	days	AU		W/m^2	AU	AU	AU	AU	%	%		m/s
GJ 3323 c	$2.31^{+0.5}_{-0.49}$	1.28	40.54	0.126	0.17	230.5	0.043	0.054	0.107	0.112	10	23	90.3	1.5
HD 22781 b	4338.38^{+308}_{-308}	12.21	528.07	1.167	0.819	296.4	0.425	0.539	0.974	1.027	10	14	–	716.5
HD 67087 c	1541.48^{+3180}_{-1150}	12.88	2374.00	3.860	0.76	317.7	1.351	1.712	2.982	3.145	10	14	–	92.4
BD+63 1405 b	$1258.61^{+98.53}_{-98.53}$	12.86	1198.48	2.060	0.88	255.7	0.698	0.885	1.601	1.688	8	12	–	181.5
HD 29021 b	$762.79^{+63.57}_{-63.57}$	13.2	1362.30	2.280	0.459	162.8	0.599	0.758	1.345	1.419	8	11	–	55.1
HD 142022 A b	$1411.17^{+1007.52}_{-1007.52}$	12.67	1928.00	2.930	0.53	133.3	0.702	0.889	1.584	1.671	8	10	–	91.4
HD 7449 b	$161.46^{+35.28}_{-35.28}$	14.01	1255.50	2.380	0.92	253.1	0.758	0.960	1.682	1.774	7	9	–	23.6
HD 190984 b	985.27^{+}	13.01	4885.00	5.500	0.57	121.5	1.216	1.540	2.701	2.849	6	8	–	48.0
HD 217850 b	$6865.13^{+826.36}_{-826.36}$	11.97	3501.30	4.560	0.762	82.6	0.854	1.081	1.920	2.025	6	7	–	432.1
HD 80869 b	$1544.65^{+206.59}_{-92.17}$	12.78	1711.70	2.878	0.862	193.0	0.809	1.025	1.805	1.904	6	8	–	154.3
HD 219077 b	$3302.25^{+28.6}_{-28.6}$	12.29	5501.00	6.220	0.77	93.9	1.254	1.588	2.836	2.992	6	8	–	180.4
HD 108341 b	$1112.41^{+1080.6}_{-381.4}$	12.89	1129.00	2.000	0.85	131.6	0.484	0.612	1.103	1.164	5	7	–	145.3
HD 66428 b	$1018.33^{+13.67}_{-13.67}$	13.07	2263.12	3.467	0.493	137.0	0.825	1.044	1.842	1.943	5	8	–	54.1
HD 219828 c	$4640.32^{+731.01}_{-731.01}$	12.15	4682.00	5.790	0.810	107.1	1.215	1.539	2.712	2.860	5	7	–	268.9
HD 75784 c	$1792.56^{+228.84}_{-228.84}$	12.66	7900.00	8.400	0.489	112.7	1.902	2.409	4.383	4.623	3	6	–	56.4
WASP-53 c	$5196.52^{+270.16}_{-260.62}$	12.08	2840.00	3.730	0.837	33.8	0.461	0.583	1.058	1.116	3	4	–	475.7
psi 1 Dra B b	$486.28^{+31.78}_{-31.78}$	13.56	3117.00	4.430	0.4	191.2	1.212	1.535	2.680	2.827	3	8	–	20.7
HD 98649 b	$2158.07^{+168.45}_{-98.53}$	12.58	6022.97	6.570	0.86	32.6	0.761	0.964	1.699	1.792	3	3	–	145.1
GJ 3293 b	$23.54^{+0.88}_{-0.89}$	5.08	30.60	0.143	0.06	1459.2	0.121	0.154	0.299	0.315	0	100	341.2	8.6
HD 142245 b	$975.74^{+133.49}_{-133.49}$	12.83	1299.00	2.780	0	1995.2	2.642	3.347	6.076	6.408	0	100	–	24.8
HD 38801 b	$3082.32^{+182.12}_{-186.57}$	12.5	685.25	1.623	0.017	1556.7	1.334	1.690	3.020	3.186	0	100	–	195.9
K2-3 d	≤ 2.8	$1.52^{+0.21}_{-0.20}$	44.56	0.207	0	2057.6	0.207	0.262	0.499	0.527	0	100	28.7	0.7
K2-332 b	5.26	$2.15^{+0.19}_{-0.15}$	17.71	0.086	0	1571.6	0.076	0.096	0.188	0.198	0	100	16.1	3.1
K2-9 b	5.83	$2.21^{+0.53}_{-0.96}$	18.45	0.091	0	1977.3	0.090	0.114	0.222	0.234	0	100	24.5	3.1
Kepler-1058 b	7.8	$2.67^{+0.11}_{-0.32}$	110.97	0.407	0	1639.2	0.355	0.449	0.825	0.871	0	100	4.8	1.3
Kepler-1090 b	5.37	$2.21^{+0.21}_{-0.17}$	198.68	0.634	0	1645.2	0.536	0.679	1.214	1.281	0	100	3.0	0.7
Kepler-1097 b	9.59	$3.19^{+0.26}_{-0.26}$	187.75	0.601	0	1563.6	0.498	0.631	1.133	1.195	0	100	4.8	1.2
Kepler-1341 b	8.65	$2.93^{+0.42}_{-0.37}$	133.00	0.471	0	1350.8	0.373	0.472	0.867	0.914	0	100	6.2	1.3
Kepler-1362 b	6.88	$2.55^{+0.12}_{-0.19}$	136.21	0.481	0	1614.8	0.412	0.522	0.951	1.003	0	100	3.3	1.0
Kepler-1410 b	3.7	$1.74^{+0.12}_{-0.14}$	60.87	0.260	0	1835.7	0.244	0.309	0.582	0.614	0	100	4.1	0.8
Kepler-1519 b	38.51	$6.91^{+0.81}_{-0.54}$	240.80	0.742	0	1870.5	0.657	0.832	1.473	1.554	0	100	9.5	4.1
Kepler-1545 b	7.48	$2.64^{+0.22}_{-0.18}$	163.69	0.553	0	1879.9	0.503	0.637	1.144	1.206	0	100	3.9	1.0
Kepler-1549 b	6.88	$2.51^{+0.22}_{-0.2}$	214.89	0.673	0	1534.9	0.550	0.696	1.245	1.313	0	100	2.9	0.8
Kepler-1552 b	6.21	$2.41^{+0.11}_{-0.1}$	184.77	0.601	0	1509.7	0.490	0.621	1.116	1.177	0	100	3.8	0.8
Kepler-1554 b	8.13	$2.84^{+0.23}_{-0.27}$	198.09	0.627	0	1607.9	0.525	0.665	1.191	1.256	0	100	3.0	1.0
Kepler-1593 b	9.2	$3.11^{+0.3}_{-0.28}$	174.51	0.570	0	1393.8	0.451	0.571	1.034	1.091	0	100	4.0	1.2
Kepler-1606 b	5.04	$2.03^{+0.23}_{-0.15}$	196.44	0.638	0	1921.7	0.580	0.735	1.310	1.382	0	100	2.0	0.6
Kepler-1625 b	28.21	$5.94^{+0.87}_{-0.53}$	287.38	0.841	0	1591.4	0.685	0.868	1.535	1.619	0	100	5.3	2.8
Kepler-1632 b	6.34	$2.41^{+0.84}_{-0.35}$	448.30	1.190	0	1737.2	0.986	1.249	2.184	2.304	0	100	3.2	0.5
Kepler-1638 b	4.45	$1.83^{+0.33}_{-0.22}$	259.34	0.788	0	1894.5	0.699	0.886	1.565	1.651	0	100	1.6	0.5
Kepler-1653 b	5.26	$2.13^{+0.16}_{-0.23}$	140.25	0.471	0	1425.1	0.380	0.481	0.878	0.926	0	100	2.3	0.8
Kepler-1690 b	7.48	2.75 $^{+}$	234.64	0.729	0	1466.7	0.580	0.734	1.310	1.381	0	100	4.0	0.8
Kepler-1701 b	5.71	2.17 $^{+}$	169.13	0.571	0	1863.4	0.519	0.658	1.183	1.248	0	100	3.1	0.7
Kepler-1840 b	7.33	2.72 $^{+}$	131.19	0.463	0	2104.9	0.453	0.573	1.042	1.099	0	100	4.8	1.1
Kepler-1881 b	8.47	2.92 $^{+}$	159.39	0.536	0	2242.6	0.535	0.677	1.220	1.286	0	100	2.9	1.1
Kepler-22 b	6.21	$2.33^{+0.13}_{-0.13}$	289.86	0.849	0	1497.4	0.678	0.858	1.525	1.608	0	100	5.5	0.6
Kepler-298 d	6.47	$2.45^{+0.2}_{-0.2}$	77.47	0.305	0	1761.5	0.277	0.351	0.651	0.686	0	100	6.4	
Kepler-309 c	6.47	$2.46^{+0.18}_{-0.18}$	105.36	0.401	0	1949.4	0.380	0.482	0.882	0.930	0	100	4.8	
Kepler-315 c	14.53	$4.06^{+0.96}_{-0.96}$	265.47	0.791	0	2390.9	0.785	0.994	1.752	1.848	0	100	3.5	
Kepler-351 d	7.33	$2.67^{+0.19}_{-0.3}$	142.54	0.498	0	2242.7	0.494	0.626	1.123	1.185	0	100	2.8	1.0
Kepler-424 c	$2215.28^{+197.05}_{-197.05}$	12.52	223.30	0.730	0	1813.4	0.643	0.815	1.450	1.530	0	100	–	230.9

Table 1 continued

Table 1 (continued)

Name	M_p $^{\pm}$	R_p $^{\pm}$	P	a	e	Flux	R1	R2	R3	R4	CHZ	OHZ	TSM	K
	M_{\oplus}	R_{\oplus}	days	AU		W/m^2	AU	AU	AU	AU	%	%		m/s
Kepler-452 b (!)	3.47	1.59 ^{+0.23} _{-0.2}	384.84	1.046	0	1516.0	0.828	1.049	1.851	1.953	0	100	1.1	0.3
Kepler-62 e	3.51	1.58 ^{+0.05} _{-0.05}	122.39	0.427	0	1571.4	0.360	0.456	0.828	0.873	0	100	3.3	0.6
Kepler-967 c	11.81	3.58 ^{+0.15} _{-0.13}	198.71	0.629	0	1426.2	0.499	0.632	1.136	1.198	0	100	7.8	1.5
Kepler-991 b	6.47	2.49 ^{+0.13} _{-0.12}	82.53	0.320	0	1660.2	0.283	0.358	0.666	0.703	0	100	7.2	1.3
KIC 5437945 b	31.29	6.27 ^{+1.6} _{-1.6}	440.78	1.159	0	2265.4	1.083	1.372	2.390	2.521	0	100	7.7	2.5
KOI-351 h	2438.61	11.06 ⁺¹ ₋₁	331.60	1.010	0	2364.2	0.979	1.240	2.172	2.291	0	100	–	198.7
Teegarden's Star b	1.05 ^{+0.13} _{-0.12}	1.03	4.91	0.025	0.00	1568.0	0.022	0.028	0.056	0.059	0	100	140.9	2.0
TRAPPIST-1 d	0.39 ^{+0.01} _{-0.01}	0.77 ^{+0.01} _{-0.01}	4.05	0.022	0	1523.0	0.019	0.025	0.050	0.053	0	100	33.5	0.8
HD 69830 d	18.12 ⁺	4.36	197.00	0.630	0.07	2072.4	0.596	0.755	1.347	1.421	0	80	–	2.2
Wolf 1061 c	3.41 ^{+0.43} _{-0.41}	1.6	17.87	0.089	0.11	1759.4	0.083	0.105	0.205	0.217	0	75	426.4	1.9
BD-08 2823 c	104.88 ⁺¹⁰ ₋₁₀	12.51	237.60	0.680	0.19	2019.6	0.655	0.830	1.518	1.601	0	62	–	13.5
HIP 12961 b	114.42 ^{+22.25} _{-22.25}	12.8	57.44	0.250	0.17	1918.6	0.241	0.305	0.581	0.613	0	62	–	24.6
HD 164509 b	140.8 ^{+26.38} _{-26.38}	14.12	280.17	0.870	0.238	2377.4	0.857	1.086	1.911	2.016	0	60	–	13.1
HD 31527 d	11.82 ^{+1.7} _{-1.64}	3.52	271.67	0.810	0.24	2496.8	0.816	1.034	1.817	1.917	0	57	122.8	1.2
Ross 128 b	1.4 ^{+0.21} _{-0.21}	1.09	9.87	0.050	0.116	2009.9	0.049	0.063	0.123	0.130	0	55	66.1	1.4
HD 80606 b	1392.1 ^{+235.19} _{-235.19}	11.74 ^{+0.34} _{-0.34}	111.44	0.475	0.93	5623.5	0.733	0.928	1.646	1.737	0	54	–	457.4
HD 155358 c	260.62 ⁺²² ₋₂₂	13.78	391.90	1.020	0.16	2487.4	1.026	1.299	2.284	2.409	0	54	–	24.4
HIP 114933 b	616.59 ^{+63.57} _{-63.57}	13.18	1481.60	2.840	0.21	2336.2	2.934	3.716	6.774	7.145	0	52	–	28.4
kap CrB b	575.59 ^{+18.12} _{-18.12}	13.34	1285.00	2.650	0.167	2311.0	2.717	3.441	6.261	6.603	0	51	–	26.2
BD+55 362 b	228.84 ^{+25.43} _{-25.43}	13.64	265.59	0.780	0.27	2574.2	0.838	1.062	1.921	2.026	0	49	–	25.2
HD 38283 b	127.13 ^{+12.71} _{-12.71}	13.62	363.20	1.020	0.41	3346.6	1.184	1.500	2.631	2.775	0	49	–	10.1
HR 810 b	721.47 ^{+79.46} _{-79.46}	13.33	302.80	0.920	0.14	2674.4	0.944	1.195	2.089	2.204	0	49	–	57.0
GJ 414 A b	7.6 ^{+2.44} _{-2.19}	2.58 ^{+1.22} _{-0.85}	50.80	0.232	0.45	3010.7	0.279	0.354	0.666	0.702	0	48	133.5	2.0
Kepler-436 b	6.88	2.63 ^{+0.23} _{-0.24}	64.00	0.339	0.19	2364.5	0.355	0.449	0.825	0.871	0	48	4.7	1.4
GJ 3021 b	1071.09 ^{+28.6} _{-28.6}	12.96	133.71	0.490	0.511	3756.2	0.619	0.784	1.391	1.467	0	47	–	166.8
HD 171028 b	832.71 ^{+50.85} _{-50.85}	13.09	550.00	1.320	0.59	4438.4	1.798	2.277	4.027	4.248	0	44	–	60.6
Kepler-56 d	1783.03 ⁺¹²⁰ ₋₁₂₀	12.76	1002.00	2.160	0.2	2523.8	2.319	2.938	5.356	5.650	0	44	–	
HD 154857 b	778.68 ^{+34.96} _{-34.96}	13.23	408.60	1.290	0.46	3801.5	1.634	2.069	3.669	3.870	0	42	–	48.2
HD 93083 b	117.6	13.26	143.58	0.477	0.14	2461.0	0.502	0.636	1.150	1.213	0	42	–	18.4
HD 31253 b	197.05 ^{+38.14} _{-38.14}	13.96	466.00	1.260	0.3	3338.3	1.447	1.833	3.206	3.382	0	42	–	12.0
Kepler-69 c	3.47	1.68 ^{+0.34} _{-0.23}	242.46	0.640	0.14	2665.5	0.677	0.857	1.518	1.601	0	41	1.8	0.4
HD 11964 b	197.69 ⁺¹⁸ ₋₁₈	13.89	1945.00	3.160	0.041	393.3	1.308	1.657	2.965	3.128	0	41	–	10.8
GJ 1132 c	2.64 ^{+0.44} _{-0.44}	1.34	8.93	0.048	0.27	2635.9	0.054	0.069	0.135	0.142	0	40	16.5	2.7
HD 134987 b	511.71 ^{+22.25} _{-22.25}	13.38	258.18	0.810	0.23	3009.7	0.905	1.146	2.024	2.134	0	39	–	49.5
HIP 75092 b	568.92 ^{+47.67} _{-47.67}	13.3	926.40	2.020	0.42	3503.0	2.547	3.227	5.865	6.186	0	39	–	34.9
KIC 7917485 b	3750.39 ^{+254.26} _{-190.7}	12.26	840.00	2.050	0.15	3217.1	2.195	2.781	4.801	5.064	0	39	–	184.8
HD 155193 b	238.37 ^{+19.07} _{-19.07}	13.84	352.65	1.040	0.21	3151.3	1.153	1.461	2.549	2.688	0	38	–	19.3
HD 124330 b	238.37 ^{+19.07} _{-19.07}	13.94	270.66	0.860	0.34	3571.8	1.038	1.315	2.313	2.440	0	38	–	22.8
HD 75898 b	861.32 ^{+114.42} _{-114.42}	13.09	422.90	1.191	0.11	2775.4	1.260	1.596	2.802	2.955	0	35	–	63.2
HD 82943 c	622.63 ^{+14.94} _{-14.94}	13.28	220.08	0.743	0.366	3860.5	0.929	1.177	2.068	2.181	0	35	–	67.3
KOI-3680 b	613.41 ^{+60.39} _{-66.74}	10.86 ^{+0.673} _{-0.785}	141.24	0.534	0.496	4575.9	0.731	0.926	1.632	1.721	0	34	–	86.1
HD 27442 b	495.81 ^{+44.5} _{-44.5}	13.55	428.10	1.271	0.06	2338.2	1.312	1.662	3.027	3.193	0	34	–	36.7
HD 102365 b	15.89 ^{+2.6} _{-2.6}	3.95	122.10	0.460	0.34	3644.8	0.569	0.721	1.276	1.346	0	33	652.4	2.4
HD 207832 b	177.98 ^{+28.92} _{-28.92}	14	160.07	0.586	0.197	3085.7	0.663	0.840	1.484	1.565	0	31	–	20.7
HD 159243 c	603.88 ^{+41.32} _{-41.32}	13.39	248.40	0.800	0.075	2773.1	0.838	1.061	1.857	1.958	0	30	–	57.1
HD 40979 b	1484.27 ^{+108.06} _{-108.06}	12.78	264.15	0.850	0.25	3587.6	1.010	1.279	2.236	2.358	0	28	–	119.0
30 Ari B b	4392.41 ^{+572.09} _{-572.09}	12.42	335.10	0.990	0.29	3993.9	1.229	1.557	2.712	2.860	0	24	–	271.4
Kepler-441 b	3.62	1.65 ^{+0.22} _{-0.24}	207.25	0.640	0.1	296.3	0.240	0.304	0.566	0.597	0	24	3.4	0.6
HD 205739 b	435.43 ^{+22.25} _{-28.6}	13.63	279.80	0.896	0.27	3895.2	1.109	1.404	2.454	2.588	0	20	–	38.7
HD 216770 b	181.16 ^{+15.89} _{-15.89}	13.98	118.45	0.460	0.37	4256.4	0.623	0.789	1.408	1.485	0	13	–	31.0
HD 5319 c	334.67 ^{+22.88} _{-22.88}	13.7	872.20	1.930	0.183	3053.2	2.274	2.881	5.241	5.528	0	9	–	19.4

Table 1 continued

Table 1 (*continued*)

Name	M_p [†]	R_p [†]	P	a	e	Flux	R1	R2	R3	R4	CHZ	OHZ	TSM	K
	M_{\oplus}	R_{\oplus}	days	AU		W/m^2	AU	AU	AU	AU	%	%		m/s
Kepler-438 b	<i>1.94</i>	<i>1.1^{+0.16}_{-0.17}</i>	35.23	0.166	0.03	2177.4	0.171	0.216	0.415	0.438	0	7	0.8	0.6
HD 207832 c	232.02 ^{+57.21} _{-15.89}	<i>13.83</i>	1155.70	2.112	0.27	236.5	0.662	0.839	1.482	1.563	0	6	–	15.3
HD 152079 b	845.75 ^{+14.62} _{-14.62}	<i>13.12</i>	2918.92	4.187	0.532	108.7	0.880	1.114	1.959	2.066	0	4	–	40.7
Kepler-88 d	969.53 ^{+44.01} _{-44.01}	<i>12.88</i>	1403.00	2.444	0.41	148.3	0.616	0.780	1.388	1.464	0	4	–	61.0
HD 220773 b	460.85 ⁺⁹⁵ ₋₉₅	<i>13.38</i>	3724.70	4.940	0.51	114.3	1.062	1.345	2.363	2.492	0	3	–	20.0
K2-125 b	<i>5.26</i>	<i>2.13^{+0.19}_{-0.18}</i>	21.75	0.121	0.08	2388.9	0.131	0.165	0.319	0.336	0	3	19.7	1.9
HD 106515 A b	3054.35 ^{+44.49} _{-44.49}	<i>12.38</i>	3630.00	4.590	0.572	79.7	0.853	1.080	1.929	2.034	0	3	–	157.1
Wolf 1061 d	<i>7.7^{+1.12}_{-1.06}</i>	<i>2.65</i>	217.21	0.470	0.55	63.1	0.083	0.105	0.205	0.217	0	3	375.6	2.2

[†]Values in italics indicate calculated values from [Chen & Kipping \(2017\)](#)

^(!)Planet is flagged as controversial in the NEA.

Table 2. Stellar Properties.

Star Name	Stellar Mass	Stellar Radius	Eff Temp	log g	Luminosity	J	V
	M_{\odot}	R_{\odot}	K	dex	L_{\odot}		
16 Cyg B	1.08	1.13	5750	4.36	1.25	4.993	6.215
30 Ari B	1.93	1.41	6331	4.43	2.87	6.080	7.092
47 UMa	1.06	1.21	5872	4.3	1.58	3.960	5.034
55 Cnc	0.91	0.94	5172	4.43	0.57	4.768	5.951
BD-00 4475	0.81	1.12	5040	4.25	0.72	7.483	9.010
BD-06 1339	0.7	0.59	4324	4.74	0.10	7.128	9.700
BD-08 2823	0.74	1.23	4746	4.13	0.68	7.960	9.860
BD-11 4672	0.65	0.64	4550	4.64	0.16	7.651	10.030
BD-17 63	0.74	0.69	4714	4.26	0.21	7.574	9.620
BD+14 4559	0.49	0.86	4864	4.26	0.37	7.882	9.780
BD+45 564	0.81	1.16	5004	4.22	0.75	8.063	9.670
BD+49 828	1.52	7.60	4943	2.85	29.51	7.246	9.381
BD+55 362	0.91	1.42	5012	4.09	1.15	7.826	9.380
BD+63 1405	0.82	1.19	5000	4.2	0.79	7.303	8.960
GJ 1061	0.12	0.16	2953	–	0.00	7.523	12.700
GJ 1132	0.18	0.21	3270	–	0.00	9.245	13.680
GJ 1148	0.34	0.36	3287	4.87	0.01	7.608	11.939
GJ 180	0.43	0.00	3371	–	0.01	7.413	10.914
GJ 273	0.29	0.29	3382	–	0.01	5.714	9.840
GJ 3021	0.9	0.90	5540	4.7	0.66	5.366	6.590
GJ 3293	0.42	0.40	3466	–	0.02	8.362	11.945
GJ 357	0.34	0.34	3505	4.94	0.02	7.337	10.910
GJ 414 A	0.65	0.68	4120	4.65	0.12	5.764	8.310
GJ 514	0.51	0.50	3728	4.76	0.04	5.902	9.050
GJ 667 C	0.33	0.43	3350	4.69	0.01	6.848	10.602
GJ 682	0.27	0.00	3028	–	0.00	6.544	10.940
GJ 832	0.45	0.50	3472	4.7	0.03	5.349	8.660
GJ 96	0.6	0.00	3785	–	0.09	6.377	9.400
HAT-P-44	0.94	0.95	5295	4.46	0.64	11.729	13.225
HD 100777	0.83	1.04	5533	4.32	0.91	7.152	8.420
HD 10180	1.06	1.11	5911	4.39	1.35	6.246	7.330
HD 102365	0.85	0.79	5630	4.57	0.57	3.931	4.890
HD 103891	1.28	2.22	6072	3.79	6.11	5.556	6.595

Table 2 *continued*

Table 2 (*continued*)

Star Name	Stellar Mass	Stellar Radius	Eff Temp	log g	Luminosity	J	V
	M_{\odot}	R_{\odot}	K	dex	L_{\odot}		
HD 10442	1.01	1.97	4912	3.19	2.03	6.158	7.828
HD 106252	1.01	1.10	5874	4.36	1.29	6.302	7.410
HD 106270	1.39	2.66	5509	3.72	5.85	6.249	7.580
HD 10647	1.11	1.10	6218	4.62	1.41	4.791	5.520
HD 106515 A	0.97	1.62	5362	4.41	1.23	6.585	7.971
HD 10697	1.13	1.79	5600	3.96	2.83	5.386	6.283
HD 108341	0.84	0.79	5122	4.45	0.39	7.863	9.380
HD 108874	1.1	1.05	5600	4.44	0.97	7.479	8.760
HD 109286	0.98	1.09	5694	4.44	1.12	7.588	8.780
HD 111998	1.18	1.45	6557	4.19	3.49	5.300	6.110
HD 114613	1.27	2.14	5641	3.87	4.16	3.692	4.850
HD 114729	0.94	1.47	5844	4.05	2.26	5.559	6.680
HD 11506	1.24	1.34	6030	–	2.14	6.508	7.510
HD 11964	0.91	2.01	5303	3.79	2.88	5.023	6.415
HD 120084	2.39	9.12	4892	2.71	43.65	4.091	5.907
HD 124330	1.15	1.35	5873	4.24	1.94	6.712	7.880
HD 125390	1.36	6.47	4850	3.13	20.80	6.421	8.210
HD 125612	1.11	1.05	5841	–	1.15	7.179	8.310
HD 12661	1.2	1.20	5645	4.36	1.31	6.182	7.430
HD 126614	1.26	1.32	5568	4.3	1.50	7.470	8.810
HD 128356	0.65	0.85	4875	4.52	0.36	–	8.241
HD 131664	1.19	1.08	5892	4.45	1.26	6.973	8.130
HD 13167	1.35	2.39	5671	3.72	5.30	7.081	8.340
HD 132406	1.03	1.34	5783	4.2	1.80	7.250	8.450
HD 132563	1.23	1.30	6289	4.3	2.37	8.003	8.928
HD 133131 A	0.95	1.03	5799	4.39	1.08	7.256	7.660
HD 134987	1.1	1.22	5736	4.31	1.45	5.268	6.470
HD 137388	0.68	0.88	5181	4.39	0.50	7.230	8.710
HD 137496	1.04	1.59	5799	4.05	2.57	8.646	9.899
HD 13908	1.29	1.67	6255	4.11	4.00	6.497	7.520
HD 141399	1.07	1.24	5600	4.28	1.36	5.890	7.209
HD 141937	1.09	1.03	5870	4.45	1.13	6.127	7.250
HD 142022 A	0.9	1.04	5421	4.35	0.84	6.384	7.700
HD 142245	3.5	4.63	4922	3.65	11.30	5.689	7.460
HD 142415	1.07	1.04	5940	4.44	1.21	6.235	7.330
HD 147379	0.6	0.00	4156	–	0.11	5.779	8.610
HD 147513	1.11	0.97	5883	4.51	0.98	4.405	5.370
HD 148156	1.22	1.21	6308	4.56	1.78	6.688	7.690
HD 148164	1.21	1.34	6032	–	2.14	7.229	8.230
HD 152079	1.15	1.13	5907	4.37	1.40	7.984	9.180
HD 153950	1.25	1.28	6124	4.32	2.07	6.313	7.390
HD 154857	1.96	2.30	5589	4.01	4.63	5.938	7.240
HD 155193	1.22	1.35	6239	4.26	2.50	6.010	7.009
HD 155358	0.92	1.32	5900	4.16	1.90	6.158	7.280
HD 156279	0.95	0.95	5453	4.46	0.72	6.677	8.070
HD 156411	1.25	2.16	5900	4.07	5.38	5.563	6.670
HD 156846	1.38	1.90	6090	4.02	4.46	5.470	6.500
HD 159243	1.12	1.12	6123	4.55	1.30	7.581	8.650
HD 159868	1.19	2.13	5534	3.92	3.82	5.941	7.240
HD 1605	1.33	3.49	4915	–	6.46	5.850	7.520
HD 16175	1.63	1.72	5981	4.18	3.40	6.166	7.297
HD 163607	1.12	1.76	5522	3.97	2.59	6.648	8.000
HD 164509	1.12	1.11	5859	–	1.32	6.938	8.100

Table 2 *continued*

Table 2 (continued)

Star Name	Stellar Mass	Stellar Radius	Eff Temp	log g	Luminosity	J	V
	M_{\odot}	R_{\odot}	K	dex	L_{\odot}		
HD 165155	1.02	0.95	5426	4.49	0.70	8.027	9.360
HD 168443	0.99	1.51	5491	4.07	1.86	5.641	6.921
HD 169830	1.4	1.74	6299	4.1	4.59	4.974	5.900
HD 170469	1.1	1.24	5842	4.3	1.61	7.047	8.210
HD 171028	1.53	2.47	5671	3.84	5.67	6.990	8.292
HD 175167	1.37	1.75	5635	4.09	2.77	6.713	8.010
HD 17674	0.98	1.18	5904	4.34	1.52	6.449	7.535
HD 18015	1.49	3.13	5603	3.64	8.67	6.628	7.890
HD 180617	0.48	0.48	3534	4.9	0.03	5.583	9.120
HD 181720	1.03	1.50	5736	4.09	2.19	6.652	7.840
HD 183263	1.31	1.23	5948	4.37	1.70	6.782	7.860
HD 187085	1.19	1.27	6117	4.28	2.03	6.190	7.220
HD 188015	1.09	1.03	5746	4.45	1.04	7.008	8.240
HD 190647	1.07	1.38	5656	4.16	1.75	6.546	7.780
HD 190984	0.91	1.53	5988	4.02	2.69	7.671	8.760
HD 191806	1.14	1.05	6010	4.45	2.23	6.966	8.090
HD 192310	0.8	0.82	5166	4.51	0.38	4.112	5.730
HD 196050	1.31	1.42	5879	4.25	2.16	6.378	7.500
HD 196067	1.29	1.73	6017	4.24	3.73	5.417	6.510
HD 196885 A	1.28	1.31	6254	4.31	2.40	5.414	6.397
HD 197037	1.11	1.10	6150	4.4	1.55	5.772	6.823
HD 203473	1.12	1.33	5780	–	1.78	7.074	8.230
HD 2039	1.23	1.19	5945	4.38	1.59	7.912	9.000
HD 205739	1.22	1.33	6176	4.29	2.29	7.585	8.560
HD 20782	1.04	1.13	5782	4.35	1.28	6.229	7.360
HD 207832	1.05	0.89	5726	–	0.78	7.587	8.780
HD 20868	0.39	0.76	4802	4.26	0.28	8.138	9.920
HD 210277	1.01	1.07	5538	4.38	0.97	5.275	6.543
HD 211810	1.03	1.13	5652	–	1.17	7.339	8.590
HD 213240	1.57	1.51	5979	4.27	2.62	5.708	6.810
HD 214823	1.31	2.04	5933	–	4.68	6.952	8.060
HD 215497	0.87	1.08	5113	4.31	0.39	7.339	8.960
HD 216435	1.3	1.59	5999	4.15	2.93	5.008	6.030
HD 216437	1.17	1.39	5909	4.19	2.11	5.044	6.040
HD 216520	0.82	0.76	5103	4.54	0.35	5.951	7.530
HD 216770	0.74	0.93	5399	4.37	0.66	6.752	8.110
HD 217786	1.02	1.27	5966	4.35	1.89	6.685	7.780
HD 217850	1.03	1.21	5544	–	1.26	7.148	8.520
HD 218566	0.76	0.85	4730	4.46	0.32	6.824	8.600
HD 219077	1.05	1.91	5362	4	2.66	4.640	6.120
HD 219415	1	2.90	4820	3.51	4.17	7.023	8.909
HD 219828	1.18	1.61	5807	–	2.63	6.871	8.040
HD 220773	1.16	1.35	5940	4.24	2.04	6.001	7.108
HD 221287	1.25	1.13	6304	4.43	1.66	6.843	7.820
HD 221585	1.19	1.70	5620	4.05	2.64	6.157	7.457
HD 222582	1.12	1.13	5790	4.38	1.29	6.522	7.680
HD 224538	1.34	1.54	6097	4.19	2.95	7.041	8.060
HD 22781	0.75	0.72	5027	4.6	0.30	7.149	8.780
HD 23079	1.12	1.07	5974	4.43	1.31	6.030	7.120
HD 23127	1.21	1.49	5843	4.15	2.32	7.423	8.580
HD 23596	1.47	1.53	6040	4.23	2.80	6.173	7.261
HD 238914	1.47	12.73	4769	2.37	70.79	6.941	8.770
HD 24040	1.1	1.39	5776	4.2	1.93	6.279	7.515

Table 2 continued

Table 2 (*continued*)

Star Name	Stellar Mass	Stellar Radius	Eff Temp	log g	Luminosity	J	V
	M_{\odot}	R_{\odot}	K	dex	L_{\odot}		
HD 27442	1.23	2.36	4846	3.78	2.77	2.374	4.440
HD 27969	1.16	1.27	5966	4.12	1.83	6.516	7.660
HD 28185	1.02	1.03	5662	4.42	0.98	6.578	7.800
HD 28254	1.06	1.48	5664	4.12	2.19	6.395	7.690
HD 29021	0.85	0.85	5560	4.44	0.62	6.518	7.760
HD 30562	1.12	1.61	5882	4.07	2.79	4.984	5.775
HD 31253	1.7	1.75	6130	4.18	3.88	6.060	7.133
HD 31527	0.96	0.97	5898	4.45	1.20	6.373	7.490
HD 331093	1.03	1.33	5544	4.2	1.51	7.043	8.380
HD 34445	1.14	1.38	5879	4.21	2.04	6.122	7.310
HD 38283	1.37	1.49	5981	4.23	2.55	5.645	6.690
HD 38529	1.41	2.56	5541	3.77	5.55	4.905	5.928
HD 38801	1.21	2.03	5338	3.88	3.00	6.800	8.260
HD 39091	1.09	1.10	6037	4.42	1.45	4.869	5.650
HD 40307	0.77	0.85	4956	4.47	0.23	5.412	7.170
HD 40979	1.45	1.21	6165	4.43	1.90	5.742	6.755
HD 4113	0.99	1.04	5688	4.4	1.22	6.672	7.880
HD 4203	1.25	1.42	5596	4.23	1.78	7.389	8.700
HD 43197	0.96	1.00	5508	4.31	0.73	7.658	8.980
HD 44219	1	1.32	5752	4.21	1.82	6.509	7.690
HD 45350	0.98	1.26	5566	4.23	1.38	6.587	7.890
HD 45364	0.82	0.97	5434	4.38	0.57	6.748	8.080
HD 4732	1.74	5.40	4959	3.16	15.49	4.338	5.900
HD 48265	1.31	1.90	5733	3.97	3.50	6.842	8.050
HD 50554	1.04	1.02	5987	–	1.39	5.776	6.856
HD 5319	1.27	4.06	4871	3.26	8.33	6.348	8.050
HD 55696	1.29	1.52	6012	–	2.69	6.900	7.950
HD 564	0.96	1.01	5902	4.53	1.11	7.218	8.320
HD 63765	0.65	0.83	5449	4.41	0.55	6.768	8.100
HD 65216	0.87	0.93	5612	4.44	0.77	6.763	7.970
HD 66428	1.08	1.10	5773	4.36	1.21	7.044	8.250
HD 67087	1.36	1.55	6330	4.19	3.47	7.098	8.050
HD 69830	0.86	0.00	5385	–	0.60	4.953	5.960
HD 70573	1	0.84	5737	4.59	0.68	7.558	8.667
HD 7199	0.77	0.97	5371	4.35	0.70	6.664	8.060
HD 73534	1.16	2.58	4917	3.6	3.49	6.524	8.230
HD 7449	1.05	0.94	6024	4.51	1.05	6.425	7.500
HD 75784	1.26	3.40	4867	3.46	5.82	6.092	7.840
HD 75898	1.26	1.58	5963	–	2.88	6.925	8.030
HD 80606	1.15	1.04	5561	4.42	0.93	7.702	9.060
HD 80869	1.08	1.06	5837	4.18	1.17	7.259	8.480
HD 81040	1.05	0.91	5755	4.54	0.82	6.505	7.720
HD 82943	1.08	1.18	5935	4.33	1.56	5.509	6.550
HD 8535	1.13	1.19	6136	4.46	1.80	6.735	7.700
HD 85390	0.76	0.90	5186	4.41	0.53	7.012	8.540
HD 86264	1.42	1.88	6210	4.02	4.57	6.505	7.410
HD 8673	1.28	1.50	6389	4.19	3.39	5.440	6.331
HD 9174	1.03	1.67	5577	4.03	2.41	7.134	8.400
HD 92788	1.15	1.14	5744	4.39	1.27	6.131	7.316
HD 93083	0.7	1.03	4995	4.26	0.41	6.694	8.300
HD 94834	1.11	4.20	4798	3.22	8.39	5.818	7.600
HD 95089	1.54	5.08	4918	3.24	13.55	6.240	7.920
HD 96167	1.27	1.94	5733	3.99	3.65	6.926	8.090

Table 2 *continued*

Table 2 (continued)

Star Name	Stellar Mass	Stellar Radius	Eff Temp	log g	Luminosity	J	V
	M_{\odot}	R_{\odot}	K	dex	L_{\odot}		
HD 98649	1.03	1.01	5790	4.51	1.03	6.811	8.000
HD 99109	0.76	0.98	5282	4.34	0.67	7.626	9.100
HIP 109384	0.78	0.89	5180	4.43	0.51	8.157	9.610
HIP 109600	0.87	0.92	5530	4.45	0.71	7.881	9.180
HIP 114933	1.39	5.27	4823	2.99	13.80	5.564	7.250
HIP 12961	0.69	0.65	3901	4.65	0.09	7.558	10.250
HIP 14810	1.01	1.07	5544	–	0.98	7.202	8.520
HIP 5158	0.78	0.95	4962	4.37	0.11	8.280	10.160
HIP 56640	1.04	4.93	4769	2.91	11.22	6.133	7.940
HIP 57274	0.73	0.68	4640	4.71	1.55	6.958	8.970
HIP 67537	2.41	8.69	4985	2.85	41.40	5.053	6.430
HIP 67851	1.63	5.92	4890	3.15	17.54	4.479	6.170
HIP 75092	1.28	4.53	4891	3.09	10.47	5.358	7.110
HIP 97233	1.93	5.34	5020	3.26	16.00	5.671	7.340
HR 810	1.34	1.13	6167	4.46	1.66	4.750	5.400
iot Dra	1.54	11.79	4504	2.48	52.72	1.293	3.297
K2-125	0.49	0.40	3654	–	0.03	12.609	16.400
K2-18	0.36	0.41	3457	–	0.02	9.763	13.477
K2-288 B	0.33	0.32	3341	4.96	0.01	–	–
K2-3	0.6	0.56	3896	4.73	0.06	9.421	12.168
K2-332	0.27	0.28	3315	4.97	0.01	13.501	–
K2-72	0.27	0.33	3360	–	0.01	11.685	15.370
K2-9	0.3	0.31	3390	–	0.01	12.451	15.860
kap CrB	1.5	4.85	4871	3.26	11.89	3.035	4.797
KELT-6	1.13	1.53	6272	4.12	3.25	9.302	10.371
Kepler-1058	0.73	0.69	4644	4.63	0.20	13.729	15.869
Kepler-1086	0.7	0.66	4350	4.65	0.14	13.691	16.002
Kepler-1090	0.86	0.82	5321	4.55	0.48	13.596	15.310
Kepler-1097	0.82	0.79	5211	4.57	0.41	13.838	15.652
Kepler-1143	0.81	0.77	5053	4.58	0.35	13.679	15.493
Kepler-1229	0.54	0.51	3784	4.75	0.05	13.228	16.124
Kepler-1318	0.73	0.70	4598	4.62	0.20	13.514	15.531
Kepler-1341	0.79	0.72	4662	4.62	0.22	13.285	15.356
Kepler-1362	0.8	0.74	4857	4.6	0.27	14.208	16.050
Kepler-1410	0.63	0.60	4092	4.67	0.09	13.586	16.319
Kepler-150	0.97	0.91	5528	4.51	0.69	13.817	15.161
Kepler-1519	0.94	0.91	5644	4.5	0.75	13.642	15.124
Kepler-1540	0.74	0.69	4540	4.63	0.18	12.250	14.429
Kepler-1544	0.81	0.74	4886	4.61	0.28	12.480	14.287
Kepler-1545	0.84	0.80	5201	4.57	0.42	13.643	15.256
Kepler-1549	0.88	0.84	5324	4.54	0.51	13.791	15.353
Kepler-1552	0.85	0.78	5202	4.58	0.40	13.504	15.203
Kepler-1554	0.84	0.81	5297	4.56	0.46	14.367	15.930
Kepler-1593	0.81	0.77	4995	4.59	0.33	14.188	16.190
Kepler-1600	0.86	0.82	5214	4.55	0.45	14.351	16.076
Kepler-1606	0.9	0.86	5422	4.53	0.57	13.875	15.396
Kepler-1625	0.96	0.94	5677	4.48	0.82	14.364	16.227
Kepler-1628	0.55	0.52	3724	4.74	0.05	14.126	17.830
Kepler-1632	1.12	1.19	6137	4.33	1.80	12.033	13.220
Kepler-1634	0.92	0.89	5474	4.51	0.64	13.198	14.636
Kepler-1635	0.89	0.85	5347	4.53	0.53	14.345	15.820
Kepler-1636	1.01	1.02	5797	4.43	1.05	14.645	15.807
Kepler-1638	0.97	0.95	5710	4.47	0.86	13.550	14.769

Table 2 continued

Table 2 (*continued*)

Star Name	Stellar Mass	Stellar Radius	Eff Temp	log g	Luminosity	J	V
	M_{\odot}	R_{\odot}	K	dex	L_{\odot}		
Kepler-1649	0.2	0.23	3240	5	0.01	13.379	17.950
Kepler-1652	0.4	0.38	3638	4.88	0.02	13.454	16.860
Kepler-1653	0.72	0.69	4807	4.62	0.23	13.880	15.864
Kepler-1654	1.01	1.18	5597	4.3	1.23	12.281	13.497
Kepler-1690	0.94	0.86	5404	4.54	0.57	13.413	14.882
Kepler-1701	0.87	0.84	5146	4.53	0.45	13.232	14.722
Kepler-1704	1.13	1.70	5745	4.03	2.83	12.138	13.392
Kepler-1708	1.09	1.12	6157	4.37	1.52	14.429	15.823
Kepler-174	–	0.62	4880	4.68	0.20	12.791	14.530
Kepler-1840	0.77	0.80	4898	4.52	0.33	13.477	15.192
Kepler-186	0.54	0.52	3755	4.74	0.05	12.473	15.138
Kepler-1868	0.74	0.69	4658	4.63	0.20	12.224	14.157
Kepler-1881	0.81	0.87	5135	4.46	0.47	14.423	15.898
Kepler-22	0.97	0.98	5518	4.44	0.79	10.523	11.751
Kepler-283	–	0.57	4351	4.72	0.10	13.927	16.216
Kepler-296	0.5	0.48	3740	4.77	0.04	13.391	16.363
Kepler-298	–	0.58	4465	4.71	0.12	13.718	15.617
Kepler-309	–	0.72	4713	4.61	0.23	13.504	15.418
Kepler-315	–	1.04	5796	4.38	1.10	13.982	15.546
Kepler-351	0.81	0.78	5225	4.58	0.41	14.669	16.229
Kepler-419	1.39	1.74	6430	4.1	4.65	12.088	13.089
Kepler-424	1.01	0.94	5460	4.5	0.71	12.905	14.429
Kepler-436	0.73	0.70	4651	4.62	0.20	14.083	15.971
Kepler-438	0.54	0.52	3748	4.74	0.04	12.130	15.104
Kepler-440	0.57	0.56	4134	4.71	0.08	12.960	15.637
Kepler-441	0.57	0.55	4340	4.71	0.09	13.040	15.567
Kepler-442	0.61	0.60	4402	4.67	0.12	13.233	15.322
Kepler-443	0.74	0.71	4723	4.61	0.22	14.365	16.207
Kepler-452	1.04	1.11	5757	4.32	1.22	12.263	13.540
Kepler-454	1.03	1.07	5701	4.37	1.09	10.357	11.567
Kepler-539	1.05	0.95	5820	4.5	0.93	11.294	12.444
Kepler-553	0.92	0.85	5266	4.55	0.50	13.578	15.034
Kepler-56	–	4.22	4819	–	8.63	10.813	12.598
Kepler-61	0.64	0.62	4017	–	0.09	13.078	15.277
Kepler-62	0.69	0.64	4925	4.68	0.21	12.256	13.965
Kepler-68	1.06	1.26	5875	4.26	1.70	8.975	10.077
Kepler-69	0.81	0.93	5638	4.4	0.80	12.631	13.866
Kepler-705	0.53	0.51	3722	4.75	0.04	13.446	16.331
Kepler-712	0.84	0.78	5148	4.58	0.38	14.399	16.161
Kepler-88	0.99	0.90	5466	–	0.65	11.882	13.209
Kepler-967	0.84	0.80	5178	4.56	0.41	12.991	14.702
Kepler-97	0.94	0.98	5779	4.43	0.96	11.744	12.994
Kepler-991	0.64	0.61	4392	4.67	0.12	13.329	15.626
KIC 10525077	1.01	1.01	6091	4.42	1.26	14.143	15.592
KIC 5437945	1.07	1.24	6340	4.16	2.23	12.667	13.834
KIC 5951458	0.98	1.52	6258	4.08	3.18	11.640	12.836
KIC 7917485	1.63	2.11	7067	4	9.91	12.303	13.166
KIC 9663113	0.98	1.03	6065	4.42	1.29	12.823	14.027
KOI-351	1.2	1.20	6080	4.4	1.77	12.790	13.883
KOI-3680	1.01	0.96	5830	4.47	0.96	13.384	14.616
LHS 1140	0.19	0.21	2988	–	0.00	9.612	14.150
PH2	0.94	1.00	5629	4.41	0.79	11.501	12.645
Proxima Cen	0.12	0.14	3050	–	0.00	5.357	11.010

Table 2 *continued*

Table 2 (*continued*)

Star Name	Stellar Mass	Stellar Radius	Eff Temp	log g	Luminosity	J	V
	M_{\odot}	R_{\odot}	K	dex	L_{\odot}		
psi 1 Dra B	1.19	1.43	6212	4.2	2.75	5.001	5.808
Ross 128	0.17	0.20	3192	–	0.00	6.505	11.120
Ross 508	0.18	0.21	3071	5.04	0.00	9.105	14.180
Teegarden’s Star	0.09	0.11	2904	–	0.00	8.394	15.130
TOI-1227	0.17	0.56	3072	–	0.00	11.890	16.999
TOI-2257	0.33	0.31	3430	4.97	0.01	11.470	15.211
TOI-2285	0.45	0.46	3491	–	0.03	9.860	13.403
TOI-700	0.41	0.42	3461	4.8	0.02	9.469	13.151
TRAPPIST-1	0.09	0.12	2566	5.24	0.00	11.354	17.020
WASP-41	0.93	0.87	5545	4.53	0.64	10.096	11.632
WASP-47	1.04	1.14	5552	4.34	1.11	10.613	11.936
WASP-53	0.84	0.80	4953	4.55	0.34	10.959	12.591
Wolf 1061	0.29	0.31	3342	–	0.01	5.950	10.100

^(!)Planet is flagged as controversial in the NEA.

Table 3. Circumbinary HZ Planet Properties.

Planet Name	M_p [†]	R_p	P	a	e	$M_{*,A}$	$R_{*,A}$	$T_{\text{eff}, A}$	log g_A	$L_{*,A}$	J_A	$M_{*,B}$	$R_{*,B}$
	M_{\oplus}	R_{\oplus}	days	AU		M_{\odot}	R_{\odot}	K	dex	L_{\odot}		M_{\odot}	R_{\odot}
Kepler-16 b	105.84 ^{+5.09} _{-5.09}	8.27 ^{+0.029} _{-0.029}	228.78	0.705	0.0069	0.69	0.65	4450	4.65	0.15	9.815	0.2	0.23
Kepler-47 c	3.17 ^{+2.18} _{-1.25}	4.65 ^{+0.09} _{-0.07}	303.23	0.9638	0.044	0.99	0.93	5611	4.50	0.89	13.97	0.85	0.87
Kepler-453 b	<i>31.95</i>	6.07 ^{+0.039} _{-0.039}	240.50	0.790	0.0359	0.94	0.83	5527	4.57	0.58	12.349	0.86	0.77
Kepler-1647 b	483.00 ⁺²⁰⁶ ₋₂₀₆	11.62 ^{+0.138} _{-0.138}	1107.59	2.721	0.0581	1.22	1.79	6210	4.02	4.28	12.376	0.882	1.464
Kepler-1661 b	17.00 ⁺¹² ₋₁₂	3.79 ^{+0.06} _{-0.06}	175.06	0.633	0.057	0.84	0.76	5100	4.66	0.35	12.729	0.26	0.28

[†]Values in italics indicate calculated values from [Chen & Kipping \(2017\)](#)

4. DISCUSSION

4.1. *Demographics*

The mass and radius histograms of the Rocky-OHZ planets (dark green), 100%HZ planets (medium green), > 0%HZ planets (light green), and the full catalog of planets from the NEA (gray) are shown in Figure 2. Histograms on the left include only those planets who have measured values for mass or radius. Histograms on the right include both measured values and calculated values using the mass-radius relationship from [Chen & Kipping \(2017\)](#). Central values were used when each planet was placed in a bin, uncertainty measurements were not used to determine bin placement for any of the histograms of Figures 2 and 3.

The side-by-side comparison of the distribution of planets with only measured values versus that with a combination of measured and calculated values highlights a bias in the mass-radius relationship, where massive planets tend to be grouped in the Jupiter radius bin.

There is a smaller fraction of low-mass planets with measured masses which is noticeable when comparing the distribution of planet masses in Figure 2A, which includes only planets with measured masses, to Figure 2B, which also includes planet masses derived from planet radius. This reflects a bias due to the difficulty in measuring the masses of small planets.

The distribution of planets in the HZ largely follows that of the full catalog of planets, with the Kolmogorov-Smirnov tests performed on Figure 2A indicating that the populations of the full catalog and the 100% HZ planets came from the same distribution (p-value = 0.608). There is a slight skew towards larger mass planets of the HZ groups. This is likely due to observational bias, with larger planets being more easily detected further away from their star.

There is a noticeable gap in the planet mass data in each population, with a peak at $\sim 10 M_{\oplus}$ and another at $\sim 400 M_{\oplus}$. Similarly, there are two distinct populations of planet radii with a peak at $\sim 2 R_{\oplus}$ and another at $\sim 13 R_{\oplus}$ in each of the groups of HZ planets and

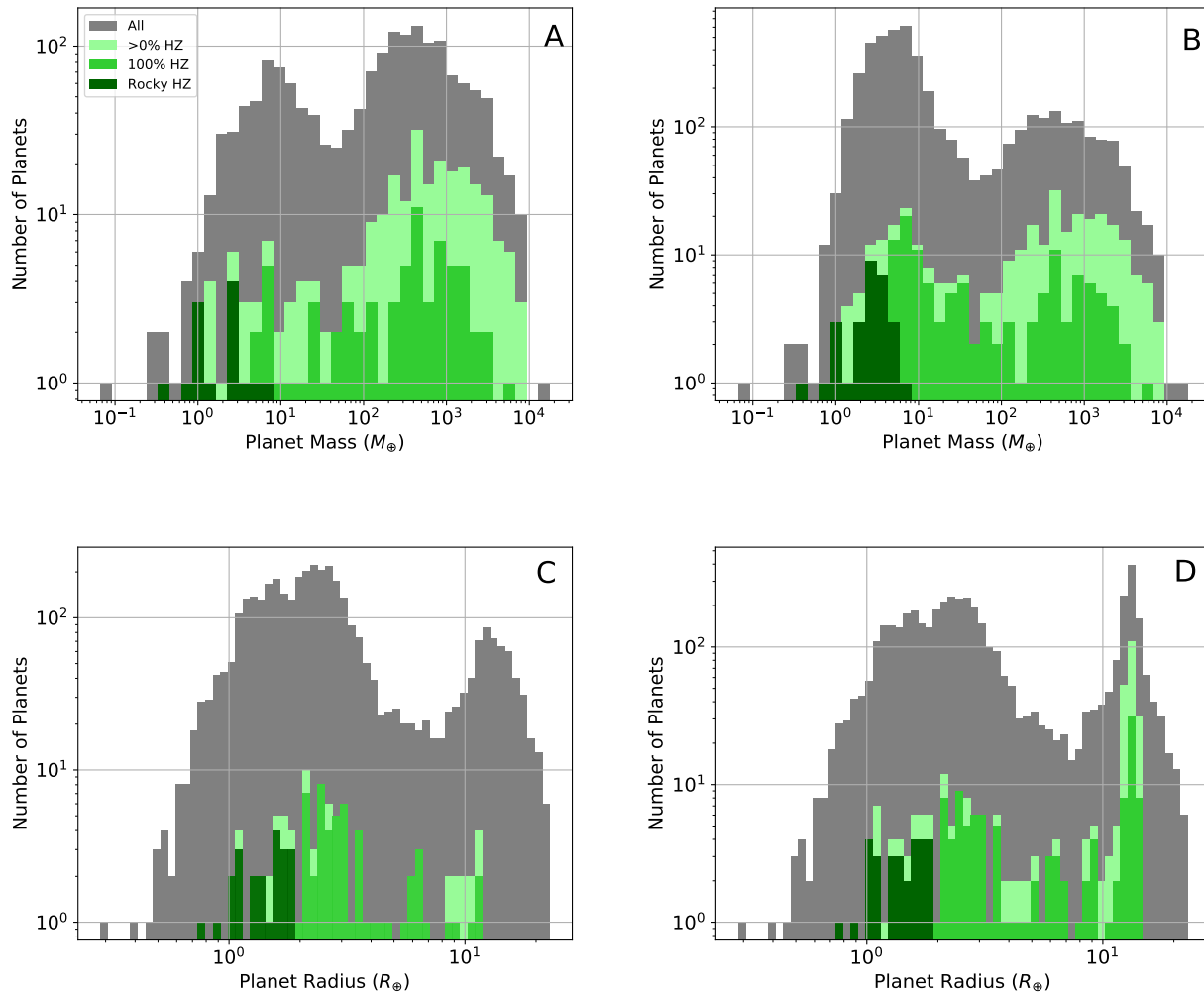


Figure 2. Mass and radius histograms of the full catalog of exoplanets from the NEA (gray), planets that spend any time at all in the HZ ($>0\%HZ$) (light green), planets found to orbit in the HZ 100% of the time (100%HZ) (medium green), and those $< 2R_{\oplus}$ that orbit in the HZ 100% of the time (Rocky-OHZ) (dark green). Histogram A includes only those planets who have measured values for mass. Histogram B includes both measured values and calculated values of mass using the mass-radius relationship from [Chen & Kipping \(2017\)](#). Histogram C includes only those planets who have measured values for radius. Histogram D includes both measured values and calculated values of radius.

the full catalog of planets. This apparent gap could be attributed to the inherent difficulty of detecting these planets that are typically far out from their host stars, and so rely on detection techniques that are more sensitive to the associated orbital period regime, such as microlensing and direct imaging ([Suzuki et al. 2018](#)). Other theories suggest this dearth of sub-Saturn planets could be attributed to core accretion theory ([Ida & Lin 2004](#)), where planets that reach $10 M_{\oplus}$ enter a runaway accretion period and rapidly grow to $\geq 100 M_{\oplus}$, provided there are sufficient materials available. The existence of this gap is still debated within the literature, such as the work by [Bennett et al. \(2021\)](#) that

contests the assertion by [Mayor et al. \(2011\)](#) and [Emmenhuber et al. \(2021\)](#) that the sub-Saturn valley does exist, showing evidence it was missing from their reanalysis of RV planets observed using CORALIE/HARPS. The gap in our data is also present amongst the HZ planets, where the RV signature of a $\geq 10 M_{\oplus}$ exceeds the limit of current technology for most stars (around a sun-like star this would create a signal of $K \sim 1 m/s$, with a larger signal for the same planet around smaller stars), however without a more thorough analysis of the observational biases that affect the detection of these planets we cannot say whether this gap is real.

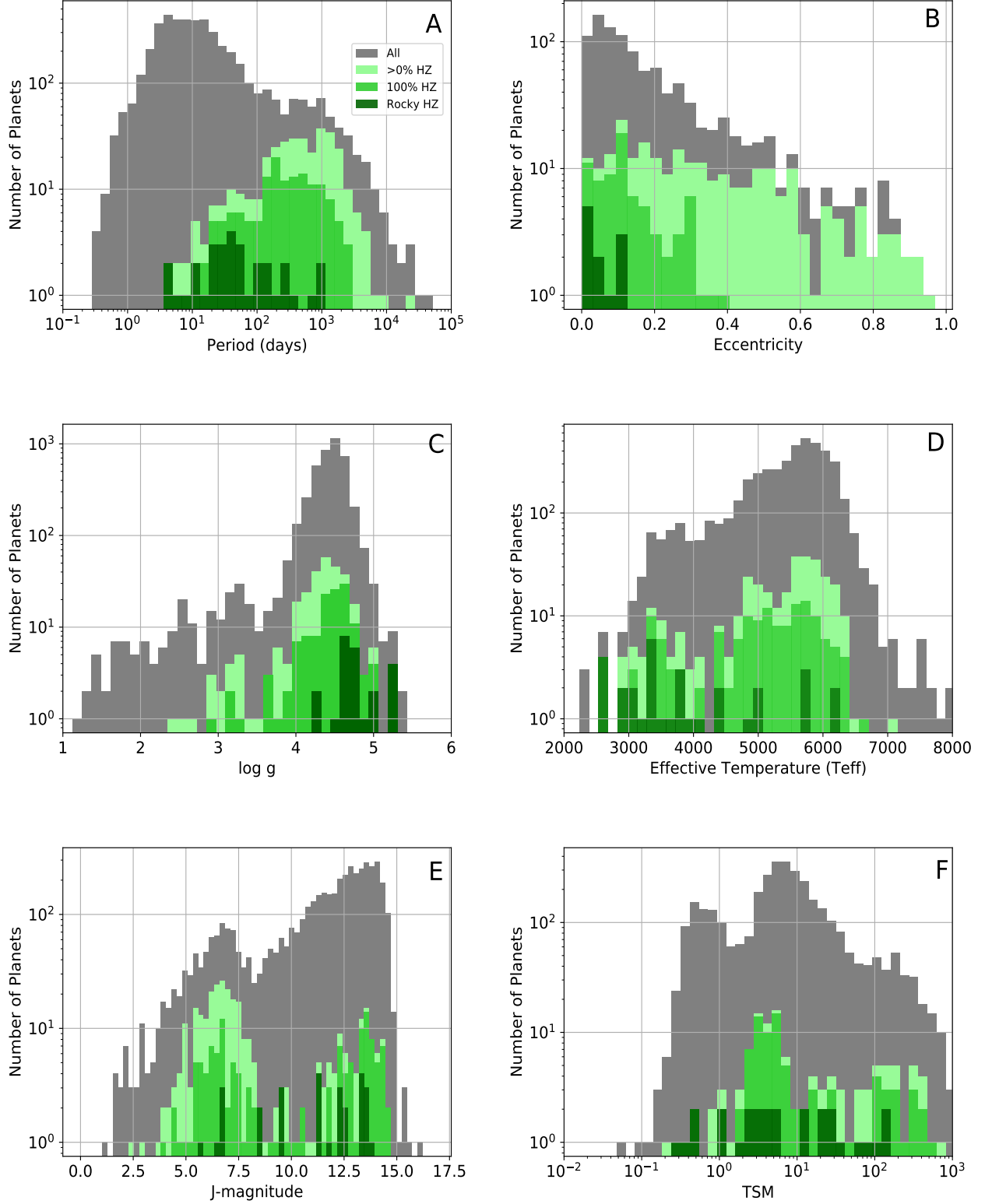


Figure 3. Histogram coloring is the same as Figure 2. Each histogram includes all planets from the NEA (gray), as well as all planets included in each of the 3 HZ groups (greens)

. A: Distribution of planet period. The HZ planets peak at higher periods than the full catalog. B: Eccentricity distribution. Only those planets with eccentricity uncertainty measurements are included in these plots. The $< 2R_{\oplus}$ planets tend to have more circular orbits. C: $\log g$ distributions. The HZ planet groups skew right progressively. D: Effective temperature (T_{eff}) distributions. The $< 2R_{\oplus}$ planets tend to be found around stars with lower T_{eff} . E: J distributions. The $> 0\%$ HZ that pass through the HZ are more often found around brighter stars. F: TSM distributions. HZ planets have lower TSM values than the full catalog.

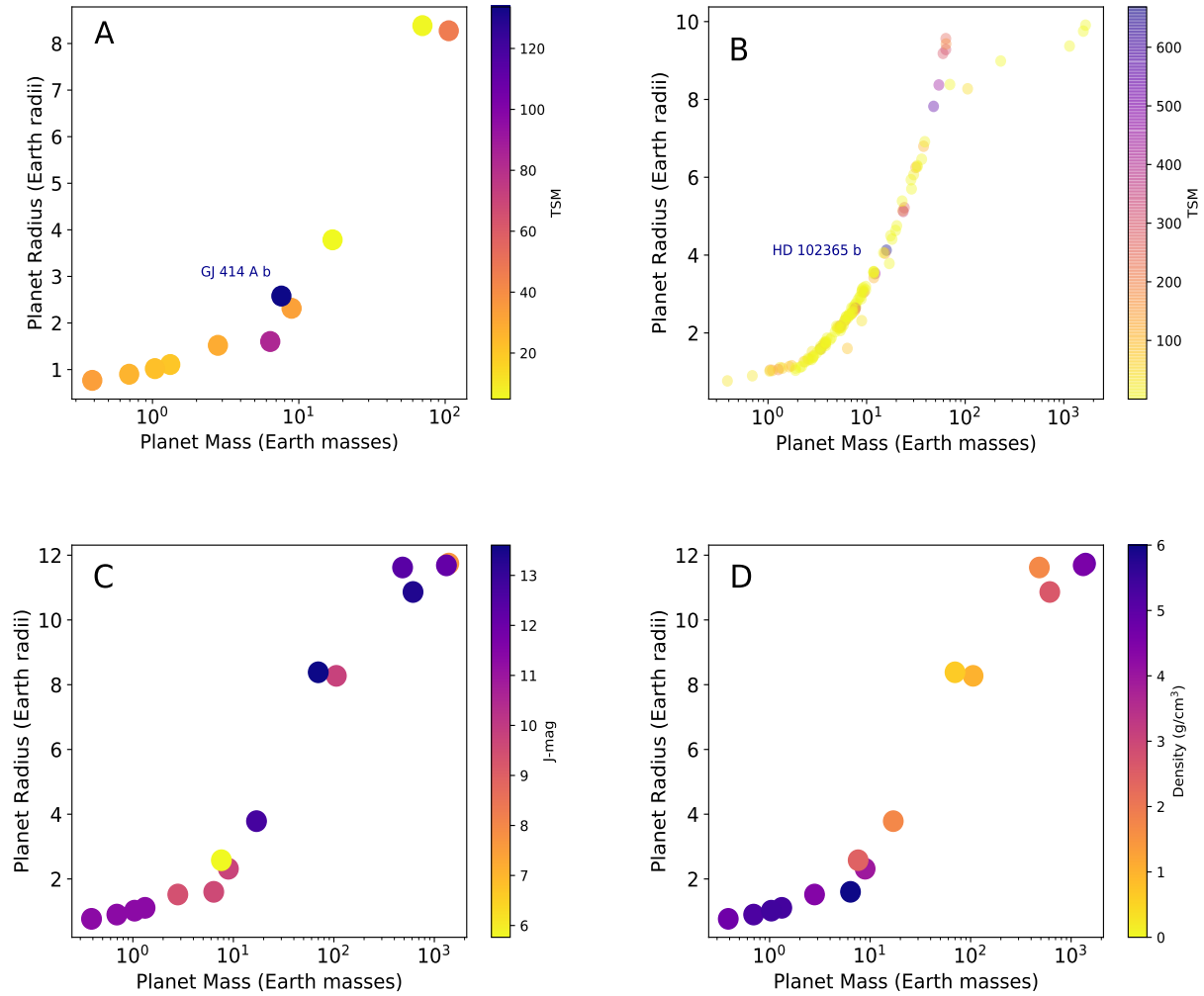


Figure 4. Figures A, C and D include only the planets found in the HZ that have both a measured mass and radius. Figure B also includes mass or radii calculations from [Chen & Kipping \(2017\)](#). A and B: Color of data points indicate transmission spectroscopy metric (TSM) of the planet ([Kempton et al. 2018](#)). The planets with the highest TSM value in each plot are labelled: GJ 414 A b, and HD 102365 b. C: Color of data points indicate J as indicated by the color bar on the right. The brightness of GJ 414 A contributed to the high TSM value. D: Color of data points indicate bulk density of the planet in g/cm^3 . The planets with the greatest density on the bottom left are the TRAPPIST-1 planets.

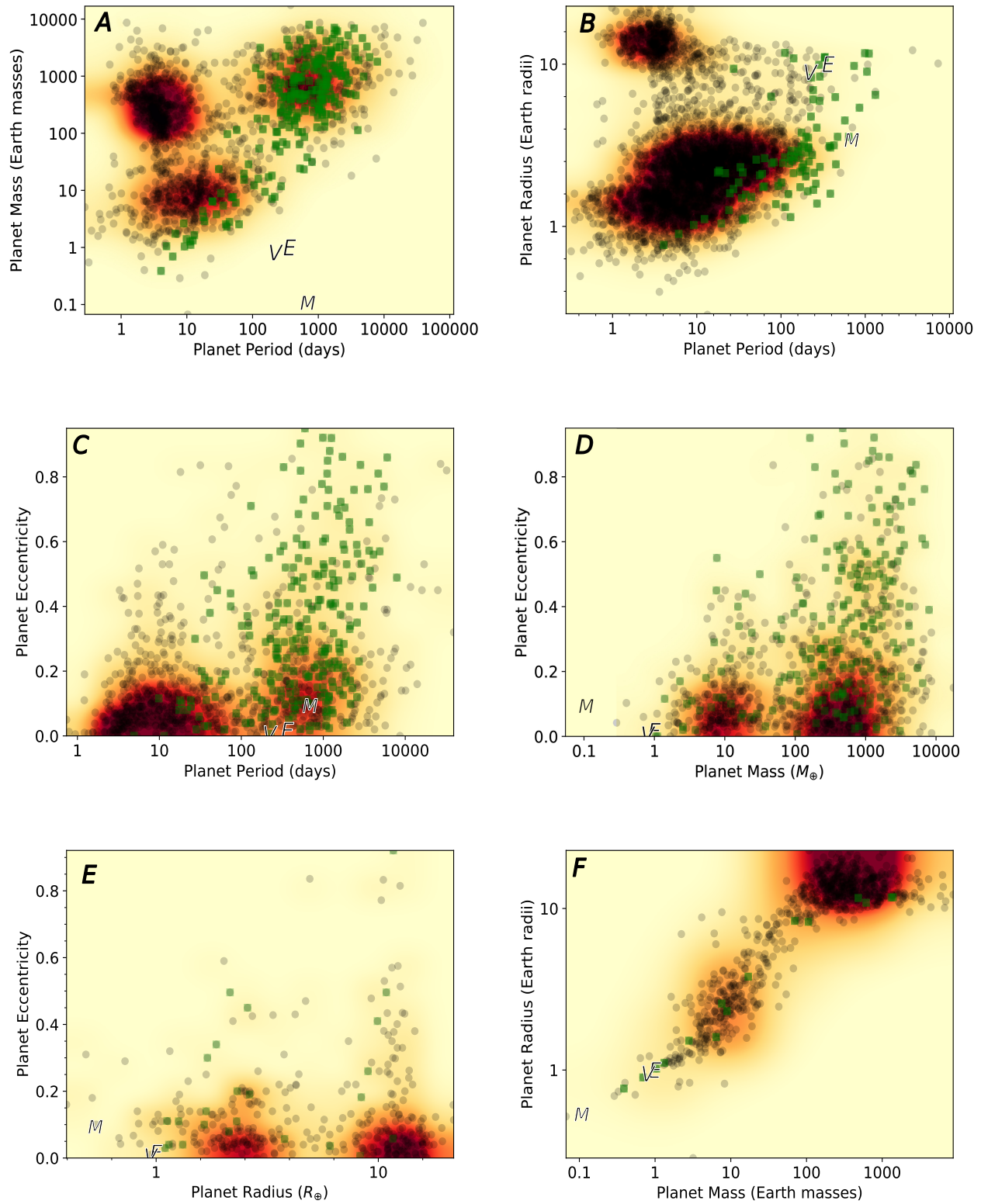


Figure 5. Heat maps with HZ planets (green) overlaying the full catalog of known exoplanets (gray). Top left: Compared to the full catalog, HZ planets tend to have longer periods and larger masses. Top right: The planet period vs radius heat map highlights the gap between the mini-Neptune sized planets and the larger Jupiter sized planets. Middle left: Longer period planets tend to have a wider distribution of eccentricity in both the full catalog and HZ planets. Middle right: So too do the larger mass planets. Bottom left: This trend of larger planets having a broader range of eccentricities is not seen in the HZ planets in the Radius-eccentricity plot, but this may be due to a smaller population. Bottom right: The measured mass versus radius plot reveals clusters of Jupiter-sized planets and Super Earths in the full catalog but not in the HZ planets.

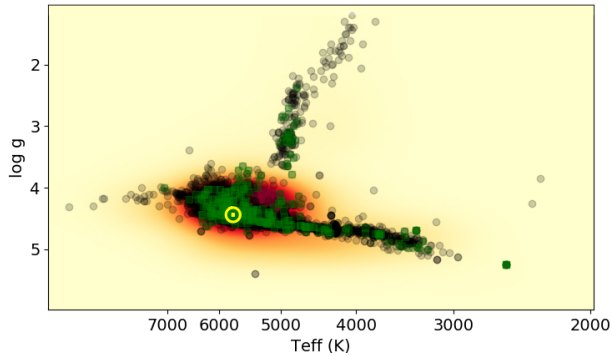


Figure 6. Heat maps of stellar effective temperature and $\log g$. The population of $> 0\%$ HZ planets span the same distribution of T_{eff} and $\log g$ as the full catalog of planets, except for amongst the more evolved stars at the top of the plot. These stars either may not host planets in the HZ, or the properties of these stars may mean detection of any HZ planets is beyond current capabilities.

It should also be noted that the peak of planets at $\sim 2 R_{\oplus}$ should not be taken as an indication of the actual peak of smaller radius planets. Many studies have shown that the number of planet occurrence rates increases to smaller sizes and so this peak is more an indication of the limits of current observational tools rather than the true distribution of smaller planets (Wittenmyer et al. 2011; Kane et al. 2016; Fulton et al. 2017; Hill et al. 2018).

There is a dip in planet occurrence around the small planet radius gap, or Fulton gap (Lopez & Fortney 2013; Owen & Wu 2013; Fulton et al. 2017) in panels C and D of Figure 2 at $\sim 1.8 R_{\oplus}$ in the full catalog and $\sim 1.1 R_{\oplus}$ within the HZ planets. The sample of planets used in Fulton et al. (2017) were restricted to orbital periods shorter than 100 days, bright stars ($K_p \leq 14.2$), with T_{eff} between $4700 \text{ K} < T_{\text{eff}} < 6500 \text{ K}$, impact parameters $b \leq 0.7$, and no giant stars. As a result, few HZ planets were included in the Fulton et al. (2017) study. However, the Fulton gap may be present in the radius distributions shown in panels C and D of Figure 2, both for the full catalog of planets as well as the $> 0\%$ HZ and 100% HZ planetary radii distributions. A recent study by Gupta & Schlichting (2019) predicted that the upper boundary of the super-Earth planet radii sat $\sim 1.1 R_{\oplus}$ at 100 days orbital period. Using the scaling law from the paper (Equation 13 of Gupta & Schlichting (2019)) this can be extrapolated to estimate a super-Earth planet radii upper boundary of $\sim 1 R_{\oplus}$ at 300 days. This prediction matches the gaps found in our data, which is close to $\sim 1.1 R_{\oplus}$ in the HZ groups. However, it must be noted that due to small number statistics and the absence of any correction for detection biases and completeness,

we are unable to provide a firm conclusion regarding whether the observed gap in the HZ is a reflection of true planetary occurrence rates or observational biases. For example, recent studies of occurrence rates around FGK stars by Kunimoto & Matthews (2020) and Hsu et al. (2019) found no evidence of the above described radius gap continuing to longer periods. Thus, further study into whether this gap exists in the HZ is essential as it will contribute to the discussion of whether this size bi-modality is caused by photoevaporation, where energy from the host star heats the upper atmospheres of the planet inducing a hydrodynamic outflow, or by core-powered mass-loss, where internal energy from the planet leftover from formation is released into the atmosphere and radiated away causing a hydrodynamic outflow, or by a combination of the two (Rogers et al. 2021; Lammer et al. 2003; Murray-Clay et al. 2009; Ginzburg et al. 2018; Gupta & Schlichting 2019). In particular, atmospheric loss processes play an important role in the initial conditions and ongoing evolution of terrestrial planet surface conditions (Dong et al. 2017). Given the distance of HZ planets from their star, core-powered mass-loss is the likely contributor to the small planet radius gap within the HZ, if proven to exist. The possibility of significant photoevaporation contributing to this radius gap amongst the HZ planets, however, would have significant implications for the atmospheric evolution of HZ planets and is worth investigating.

It is evident that more of the larger mass planets, and to a lesser extent, more of the larger radius planets, are being excluded from the 100% HZ group than smaller mass or radius planets. The planets being excluded from the 100% HZ group are also the longer period planets with higher eccentricities (Figure 3). This hints that the initial origin of these giant planets was beyond the snowline, and migration or planet scattering likely led to their current positioning.

Histograms of the distribution of planet period, eccentricity, stellar effective temperature, $\log g$, and J are shown in Figure 3. In order for liquid water to exist on the surface of a planet, it cannot orbit too close to the star. For that reason the right skew of the peak of the HZ planets period compared to the full catalog was expected. The expected period distribution peak for the HZ planets was in the hundreds of days due to the focus of missions like Kepler on sun-like stars. Considering the star type of each group peaks around G-type stars, the $> 0\%$ HZ planets peak at ~ 1000 days orbital period was higher than was initially anticipated. This is due to the inclusion of all planets that spend any amount of time in the HZ; long period eccentric planets that pass through the HZ contribute significantly to skewing the period

distribution towards longer periods. For the 100%HZ planets, the distribution moved towards smaller periods with a peak of ~ 200 days.

As noted earlier, the planets being excluded from the 100%HZ group are planets with higher eccentricities, as seen in the eccentricity histogram of Figure 3. The orbits of planets with high eccentricity will cover a wide range of distances from the star and so are likely to pass through a particular area around the star like the HZ provided their orbital period is long enough. Thus the flat distribution of the $> 0\%$ HZ planets eccentricity is to be expected. Once the selection was refined to only the 100%HZ planets it could be seen that the distribution more closely resembles that of the full catalog. As smaller planets have been shown to prefer circular orbits (Kane et al. 2012; Van-Eylen & Albrecht 2015), the low eccentricities of the Rocky-OHZ planets is expected.

The peak of the TSM distribution for the HZ planets is in the middle of the gap for the full distribution. These low TSM values for HZ planets are likely driven by the T_{eq} of these temperate planets.

Of the remaining histograms in Figure 3, there is a valley of planets found around K stars ($T_{\text{eff}} \sim 4000$ K), particularly within the HZ. This is likely due to observational biases; target selection of RV surveys peak around solar type stars as the spectral lines of G-type stars are ideal for RVs. Later type stars have increased activity and earlier type stars lose the spectral lines that the RV method relies on (Vanderburg et al. 2016). Stellar rotation periods and associated activity signals can often peak throughout the orbital period range in the HZ of M dwarf stars, creating an additional source of uncertainty for later type stars (Vanderburg et al. 2016). Transit studies on the other hand peak at M-dwarf stars as transit surveys are biased towards short period planets due to the necessity of detecting multiple transits for confirmation (Batalha et al. 2010). Planets transiting M-dwarf stars are also easier to find because of relatively large planet-to-star radius ratios allow greater transit depths for the same planet size.

To demonstrate the bias toward detecting HZ planets around M-dwarf stars with the transit method, we looked at the breakdown of HZ planet detection with the Kepler mission. We adopted a cutoff from Dressing & Charbonneau (2013) of $T_{\text{eff}} < 4000$ K to determine which stars were M-dwarfs within Tables 1 and 2, with $\log g > 4$ to ensure only main sequence stars were selected. We found 9 of the 86 ($\sim 10\%$) Kepler planets in our tables are found to orbit within the HZ of M-dwarf stars, despite the fact that M-dwarf stars constituted only $\sim 2\%$ of the Kepler stellar sample Berger et al. (2020). This bias is even more extreme

for the smallest planets, which are near or below the limit of detectability with the transit method. We find $\sim 39\%$ of Kepler HZ planets with radii $\leq 2 R_{\oplus}$ orbit M-dwarf stars. Bias-corrected occurrence rate estimates from Kepler have shown similar HZ abundances for M and F,G,K dwarf stars (Dressing & Charbonneau 2015; Bryson et al. 2021), indicating that the over-inflation of M-dwarf planets in our Kepler sample is predominantly due to observational biases.

The gap in the J distribution around 8.5-9 magnitude for each population is again due to observational biases. As transit surveys try to simultaneously observe a large number of stars in their field of view, transit host stars tend to be very faint. RV host stars on the other hand tend to be bright, with only a handful facilities performing well on stars fainter than 9th magnitude. The peak of HZ planets around fainter stars is smaller than that of the full catalog. This is an indication that planets in the HZ of dim stars are difficult to find due to the reduction in detectability via some methods like RV and transits with distance from the star.

Figure 4 includes mass-radius scatter plots colored with a third parameter: TSM, J or density. Plots A, C and D include only the planets found in the HZ that have both a measured mass and radius. Plot B also includes planets with mass or radius calculated by the method in Chen & Kipping (2017). The color of data points on the top row of Figure 4 indicate TSM of the planet (Kempton et al. 2018). On the left, one planet with both measured mass and radius stands out as having a significantly higher TSM value than the other planets: GJ 414 A b, a sub-Neptune planet that spends 48% of its orbit in the OHZ initially discovered by Dedrick et al. (2021). On the right, HD 102365 b, a Neptune-like planet discovered by Tinney et al. (2011) that spends 33% of its orbit within the OHZ, has the highest TSM value of all the planets in the HZ list.

In plot C the color of data points indicate J . The brightest star of the measured values is GJ 414 A. This brightness contributed to the high TSM value of the planet orbiting this star.

Plot D of Figure 4 includes data points colored to the corresponding bulk density of the planet in g/cm^3 . The planets with the greatest density of all the planets with both mass and radius measurements are the Trappist-1 planets d, e, f and g seen at the bottom left of the plot.

Figures 5 and 6 include scatter plots of the entire exoplanet catalog (gray) versus the $> 0\%$ HZ planets (green). If the plot includes mass, radius or eccentricity, only planets with measured values for each are included. These plots also include a heat map to allow easy identification of clusters and their relative density.

Plot A of Figure 5 shows planet period versus planet mass. There are three clusters of planets in the full catalog: Hot Jupiters at the top left, cool Jupiters at the top right and hot super Earths at the bottom left. Of the $> 0\%$ HZ planets, there is a large cluster of cool Jupiter planets and then a smaller cluster of warm super Earths and terrestrial planets. This plot highlights the relationship between the size of the planet and the stellar type, as the HZ of smaller stars is closer than larger stars and thus the period of HZ planets orbiting M-dwarfs is smaller than those orbiting larger stars. Within the population of HZ planets shown in the plot, no giant planets appear in the HZ around smaller stars. As giant planets will have a greater gravitational effect on smaller stars, if these planets did exist there is a high likelihood they would have been detected. These results are in line with previous studies that calculated lower occurrence rates of giant planets around low mass stars than higher mass stars due to the lack of planet building materials (Montet et al. 2014; Bowler et al. 2015; Hill et al. 2018). While the plot also suggests that larger stars tend to host more massive planets in the HZ, this is likely influenced by the increased difficulty encountered when trying to detect lower mass planets around larger stars.

Plot B of Figure 5 shows planet period versus planet radius. There are two major clusters in the full catalog which show the sub-Saturn valley (Ida & Lin 2004; Suzuki et al. 2018), but as is mentioned earlier in this section, this gap may be attributed to the inherent difficulty of finding these types of planets, particularly by both the transit and RV detection methods which dominate the detection of exoplanets to date. Similarly to the period vs mass plot, smaller HZ planets tend to be found around smaller stars.

Plots C, D and E of Figure 5 show eccentricity versus planet orbital period, mass and radius respectively. Longer period and larger mass planets tend to have a wider range of eccentricities than the short period, low mass planets. The closer to the star and the less massive a planet is, the more likely the gravitational pull of the star will force the planet's orbit to circularise. This is seen to some extent in the radius vs eccentricity plot as well, though less strongly amongst the HZ planets due to the small number of planets with measured radii in the $> 0\%$ HZ group.

Plot F of Figure 5 shows planet mass versus radius of all the measured planets. The mass radius relation is evident, the HZ planets follow the full catalog of planets along the mass-radius relationship, and two main clusters are present: massive Jupiter planets in the top left and Super Earths in the middle of the plot.

In the stellar effective temperature vs $\log g$ plot of Figure 6, the $> 0\%$ HZ planets span the same distribution of T_{eff} and $\log g$ as the full catalog, except for amongst the more evolved stars. These stars may not host planets in the HZ, or the properties of the stars may mean detection of any HZ planets is beyond current capabilities. As these stars grow the transit depth of existing planets will reduce making it more difficult to detect transiting exoplanets, and RV surveys tend to focus on main sequence stars rather than highly evolved stars.

4.2. Extreme cases in the Habitable Zone

Here we highlight some of the extreme cases in the catalog of HZ planets and discuss how their unique attributes may affect the habitability on these planets. Future observations of these planets will allow testing of these hypotheses and further refinement of the HZ boundaries.

4.2.1. Eccentric Planets

Many studies have proposed that planets that are temporarily outside the HZ can maintain or regain habitable periods (Williams & Pollard 2002; Kane & Gelino 2012a; Way & Georgakarakos 2017; Palubski et al. 2020; Kane et al. 2021). Observations of more eccentric HZ planets will help test the boundaries of habitability and the effect of eccentricity on planets orbiting within or passing through the HZ.

The highest eccentricity planets in and passing through the HZ are shown in Figure 7. The most eccentric planet within the CHZ is KELT-6 c, a $3.71 \pm 0.21 M_J$ planet orbiting 100% in the CHZ of a F8 star (Collins et al. 2014). With an eccentricity of 0.21, this planet's T_{eq} will range from 385 K at periastron to 311 K at apastron. The most eccentric planet within the OHZ is GJ 1148 b, which spends 100% of the time in the OHZ and 83.9% in the CHZ. Discovered by Haghighipour et al. (2010), GJ 1148 b is a $0.3043^{+0.0044}_{-0.0032} M_J$ planet orbiting a M4V star. With an eccentricity of 0.38 this planet's T_{eq} will range from 422 K at periastron to 283 K at apastron. The most eccentric planet to pass through the HZ is also the most eccentric planet to be found to date: HD 20782 b (Jones et al. 2006). This $1.4878^{+0.1045}_{-0.1066} M_J$ planet orbiting a G3V star has an extreme 0.95 eccentricity, causing a massive variation in T_{eq} of 1603 K at periastron to 257 K at apastron. Kepler-296 f is the most eccentric $\leq 2R_{\oplus}$ planet that spends 100% of its orbit in the OHZ of an M2 V star (Rowe et al. 2014; Muirhead et al. 2012). With an eccentricity of 0.33 this planet undergoes fluctuations in T_{eq} between 303–427K. GJ 1061 d, a $1.64^{+0.24}_{-0.23} M_{\oplus}$ planet, is the most eccentric terrestrial planet that passes through

the HZ of an M5.5 V star (Dreizler et al. 2020). With an eccentricity of 0.53, GJ 1061 d spends 87% of its orbit in the OHZ and the remaining 13% interior to the zone. The range of T_{eq} that GJ 1061 d undergoes is 278-502K.

4.2.2. Giant Planets

The most massive planets ($\leq 13 M_J$) in the HZ are HD 106270 b, a $10.13 \pm 0.27 M_J$ planet orbiting 100% within the OHZ of a G5IV sub-giant star (Johnson et al. 2011) and HD 38529 c, $12.99 \pm 0.15 M_J$ planet that spends 56.8% in the OHZ of a G8III, slightly evolved star (Fischer et al. 2001). While giant planets are not considered habitable themselves, they may be host to large, terrestrial exomoons. These moons could then benefit from the reflected light and emitted heat from the planet, as well as tidal heating from the motion of the moon around the planet (Heller & Barnes 2013). With all this on top of the flux received from the host star, a moon orbiting a planet like HD 38529 c, which spends part of its orbit exterior to the HZ, may have an increased chance at maintaining habitable conditions than a lone planet on a similar orbit would (Heller & Barnes 2013; Heller & Armstrong 2014; Hill et al. 2018). Note that we use a conservative upper limit on giant planet mass of $\leq 13 M_J$ in this section. This is to ensure no brown dwarfs are included in this section (see Section 4.2.3 for brown dwarfs in the HZ).

4.2.3. Brown Dwarfs

HD 214823 b is the largest brown dwarf ($20.3 \pm 2.6 M_J$) orbiting entirely within the OHZ of a slightly evolved G0 star (Díaz et al. 2016b). With 45% of its orbit within the OHZ, BD-00 4475 b is the largest brown dwarf ($25.05 \pm 2.23 M_J$) passing through the HZ of a G0 star (Dalal et al. 2021). A brown dwarf fusing deuterium will emit heat and thus have its own HZ (Belu et al. 2013). Any satellite orbiting within the HZ of a brown dwarf that is orbiting within the HZ of the its star would potentially have a prolonged period of habitability. Stars increase their luminosity as they age and so during the faint early lifetime of the star, a satellite in the HZ of the brown dwarf may rely on the brown dwarf's emitted heat until the stellar temperature increases sufficiently so that both the satellite and brown dwarf orbit within the HZ of the star. Additionally, a brown dwarf will slowly cool as it ages, but a body orbiting a brown dwarf that orbits within the HZ of the star will be able to maintain temperate conditions long after the brown dwarf has cooled.

4.2.4. High and Low Density Planets

Density was only calculated for planets that had both a measured mass and radius. Of the 13 HZ planets that

met these conditions, the highest density planets are TRAPPIST-1 f, g & e (Gillon et al. 2016). Studies into the possible composition of these planets have proposed that these are volatile rich planets (Unterborn et al. 2018). As TRAPPIST-1 is a priority target for observations with the James Webb Space Telescope (JWST), there will soon be more insight into the composition of these worlds.

The lowest density planets both within and passing through the HZ are also all circumbinary planets. These are Kepler-1661 b, Kepler-1647 b and Kepler-16 b (Socia et al. 2020; Kostov et al. 2016; Doyle et al. 2011). More about circumbinary planets in the HZ can be found in Section 4.3.

The lowest density planet that is non circumbinary is GJ 414 A b, a puffy mini-Neptune that spends 48% of its orbit in the OHZ of a K7 V star (Dedrick et al. 2021).

Observations of the atmospheres of the lowest and highest density planets within the HZ will give insight into the composition of these planets and will help in determining the density limitations of habitability.

4.2.5. Evolved Stars

Numerous planets have been found in the HZ of evolved stars (Figure 6). While these planets are currently within the HZ of their star, this will be temporary. As stars age they will increase in radius and luminosity and the HZ will move further away from the star. Planets that were once exterior to the HZ will temporarily orbit within the HZ as the star evolves and expands at the end of its life. Many of these planets will have formed exterior to the snow line, the distance from a star where lighter elements will condense (Hayashi 1981; Morbidelli et al. 2015; Lambrechts & Johansen 2014), and so may have large inventories of H_2O and other volatiles essential for the development of life. It is unclear what length of time is required for life to take hold and evolve on a planet so these planets are excellent targets for observations to determine both if life can start on a planet that spent the majority of its life exterior to the HZ, and if life can evolve to a point where a biosignature can be detected within the time the planet remains in the HZ. Additionally, as giant planets tend to form far away from the star beyond the snow line, gas giants with potentially large exomoons may exist beyond the main sequence HZ of the star. While the moon may have been able to maintain habitable conditions through tidal heating and energy emitted from the host planet, the evolution of the star and movement outwards of the HZ will allow a time in which the moon will exist in the temperate zone of the star. This may enable a period where life that had managed to take hold on the

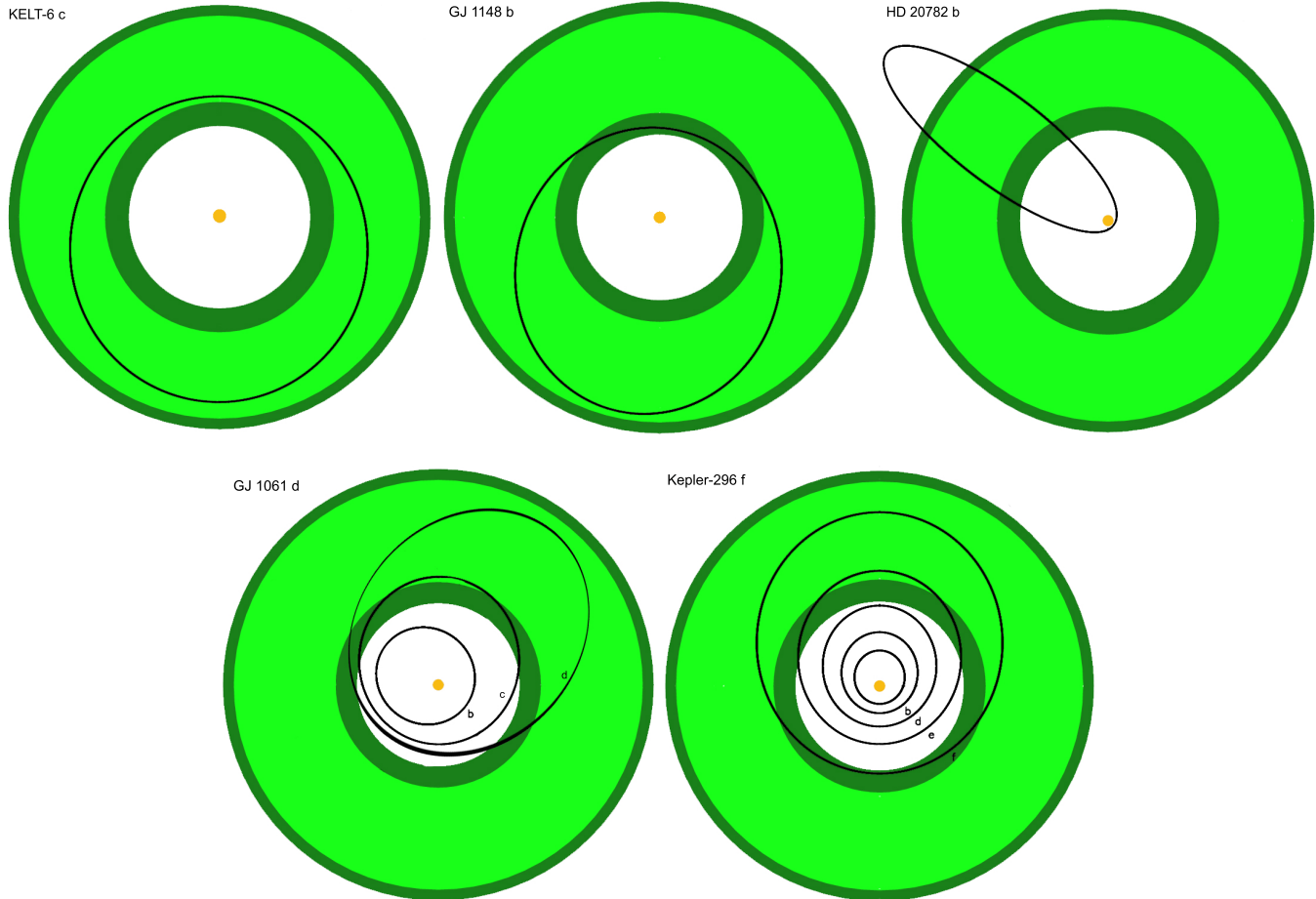


Figure 7. The most eccentric HZ planets. Top left: Most eccentric planet within the CHZ: KELT-6 c is a $3.71 \pm 0.21 M_J$ planet discovered by Collins et al. (2014). With an eccentricity of 0.21 this planet’s T_{eq} will range from 385 K at periastron to 311 K at apastron. Top middle: Most eccentric planet within the OHZ: GJ 1148 b, discovered by Haghighipour et al. (2010), is a $0.3043^{+0.0044}_{-0.0032} M_J$ planet. With an eccentricity of 0.38 this planet’s T_{eq} will range from 422 K at periastron to 283 K at apastron. Top right: Most eccentric planet to pass through the HZ: HD 20782 b, discovered by Jones et al. (2006). This $1.4878^{+0.1045}_{-0.1066} M_J$ planet is the most eccentric planet found to date and has a massive variation in T_{eq} of 1603 K at periastron to 257 K at apastron. Bottom left: The most eccentric planet $\leq 2 R_{\oplus}$ that passes through the OHZ, GJ 1061 d has an eccentricity of 0.58 and has a variation in T_{eq} of 278 – 502 K (Dreizler et al. 2020). Bottom right: The most eccentric planet $\leq 2 R_{\oplus}$ that spends 100% of its orbit in the OHZ, Kepler-296 f, has an eccentricity of 0.33 and fluctuations in T_{eq} of 303–427K (Rowe et al. 2014).

moon can now proliferate, or conversely, may destroy any existing life that is unable to adapt to the changing conditions on the moon.

There is a noticeable lack of HZ planets detected around highly evolved stars, as seen in Figure 6. As mentioned in Section 4.1, this is likely due to an observational bias.

4.3. Circumbinary Planets

The HZ boundaries of circumbinary systems has been a topic of significant interest within the habitability literature (Haghighipour & Kaltenegger 2013; Kane & Hinkel 2013; Cuntz 2014; Müller & Haghighipour 2014; Cukier et al. 2019). Such interest includes the investigation of the climate effects that the variable insolation

flux received by the planet may have upon their climate evolution (Mason et al. 2015; Popp & Eggl 2017; Wolf et al. 2020). There have been numerous CBP discoveries, particularly in the era of Kepler and TESS. The first discovery was that of Kepler-16b, a $0.333 \pm 0.016 M_J$ planet (Doyle et al. 2011) whose orbit lies along the inner edge of the HZ (Kane & Hinkel 2013). Other discoveries of CBPs that lie within the binary HZ are Kepler-47 c, a $3.17 M_{\oplus}$ planet (Orosz et al. 2012, 2019), Kepler-453 b, a $\leq 16 M_{\oplus}$ planet (Welsh et al. 2015), Kepler-1661 b, a $17 M_{\oplus}$ planet (Socia et al. 2020), and Kepler-1647 b, a $1.52 M_J$ planet (Kostov et al. 2016).

It is interesting to note that each of the three lowest density planets are all circumbinary, however the requirement within this study that the planet have both a

measured mass and radius contributes to this relationship. The masses of CBPs can be obtained through the transit timing variations (TTVs) of the binary orbit. As these star systems are eclipsing binaries, the likelihood that the planet will also transit is increased (Martin & Triaud 2015). This is due to the higher likelihood of alignment between the planet and binary star orbits due to the conservation of angular momentum. This causes an increase in the likelihood of a transit of the planet, which is typically low for planets as far out as the HZ.

For some of these CBP systems the HZ coincides with the dynamical limit of the system (Socia et al. 2020; Welsh et al. 2015), so the closest a planet can orbit the binary and remain stable happens to be within the HZ. The CBPs and their parameters are shown in Table 3.

4.4. Controversy in the Habitable Zone

Six planets included in Table 1 are listed as controversial in the NEA. HD 40307 g discovered by Tuomi et al. (2013) is refuted by Díaz et al. (2016a), who did not recover a significant signal at the expected period. KIC 5951458 b, discovered by Wang et al. (2015), has subsequently been refuted by Dalba et al. (2020) who suggests stellar multiplicity is the source of this signal. GJ 667 C e & GJ 667 C f were both discovered by Anglada-Escudé et al. (2013) and both suggested to be stellar activity by Robertson & Mahadevan (2014). Kepler-452 b, which was discovered by Jenkins et al. (2015), has since been claimed to be instrumental effects by both Mullally et al. (2018) and Burke et al. (2019). Also refuted by Burke et al. (2019) is Kepler-186 f, initially discovered by Quintana et al. (2014). As each of these planets remains in the NEA planet table they have been kept in the table of HZ planets, however we suggest caution should be exercised when following up on any of these planets.

4.5. Follow-up Opportunities

Follow-up observations of planets in the HZ are essential to determining their habitability potential, assessing the usefulness of target selection tools like HZ boundaries, and testing the habitability limits of other parameters within the HZ. Future missions like the JWST will probe the atmospheres of both terrestrial and gaseous HZ planets and provide insight to their composition.

The rocky planet from Table 1 that spends 100% of the time in HZ with the highest TSM value is GJ 667 C c, a Super Earth discovered by Bonfils et al. (2013). This is followed closely by Teegarden’s Star b, a terrestrial planet ($1.05 M_{\oplus}$) that has an orbit within the OHZ (Zechmeister et al. 2019). Each of these systems are ideal targets for future observations as they are multi

planet systems with multiple planets orbiting in the HZ. GJ 667 C is host to another two Super Earth’s that orbit within the CHZ: GJ 667 C f and GJ 667 C e (Anglada-Escudé et al. 2013), while Teegarden’s Star c is a terrestrial planet ($1.1 M_{\oplus}$) orbiting within the CHZ.

Multi planet systems are ideal targets for comparative planetology (Weiss et al. 2018). Similar historical conditions can be assumed for each planet in the system and so how the planets differences in size and distance from their star affect their surface conditions can be seen more directly. Thus comparative planetology can be much more powerful in determining the limits of habitability than comparing many single planets around multiple stars. For this reason the TRAPPIST-1 system is another great target for follow-up observations.

Of the $\leq 2 R_{\oplus}$ planets that pass through the HZ, Wolf 1061 c has the highest TSM value, followed by Proxima Cen b (Wright et al. 2016; Anglada-Escudé et al. 2016). Atmospheric observations of these planets will allow insight into how time outside of the HZ may affect the habitability of rocky planets.

Of the HZ planets that have both a measured mass and radius GJ 414 A b, a $2.57 R_{\oplus}$ planet, has the highest TSM value (Figure 3) (Dedrick et al. 2021). Of all the HZ planets, including those with a calculated mass or radius, HD 102365 b, a $15.89 M_{\oplus}$ planet, has the greatest TSM, followed by 55 Cnc f, a $47.77 M_{\oplus}$ planet (Tinney et al. 2011; Fischer et al. 2008).

Observations of the extreme planets from Section 4.2 are essential to determine the limits of habitability. In particular, observations of the more eccentric terrestrial planets would help determine the limits of temperature variation on habitability. The most eccentric terrestrial planet ($\leq 2 R_{\oplus}$) that spends 100% of its orbit in the OHZ is Kepler-296 f (Rowe et al. 2014). Kepler-296 is another multi planet system with an additional eccentric, $\leq 2 R_{\oplus}$ HZ planet that spends 64% of its orbit in the OHZ; Kepler-296 e (Figure 7). Observations that can probe the atmospheres of these planets will allow a direct comparison of the effects of eccentricity and the associated temperature changes for planets both within and passing through the HZ.

Giant planets in the HZ could host rocky exomoons that have the potential to be habitable worlds (Section 4.2.2). Recent discoveries of possible moon signals indicate we are on the cusp of being able to detect these elusive satellites (Kipping et al. 2022; Teachey et al. 2017). As well as observations to detect these moons, further RV observations of the most promising HZ giants will aid in refining their orbits. This will enable transit ephemeris refinement to allow for better targeted transit

follow-up observations to characterize these planets and search for moons.

4.5.1. *RV observations*

Very few HZ planets have both mass and radius measured. As planet bulk density is an essential measurement to aid in determining atmosphere composition, many more planets with both a measured mass and radius are needed for future transmission missions. Dedicated RV follow-up of transiting HZ planets and more projects like the Transit Ephemeris Refinement and Monitoring Survey (TERMS) (Kane et al. 2009; Pilyavsky et al. 2011; Kane et al. 2011b,a,c) are needed in order to increase the population of HZ planets that have both and measured mass and radius. Figure 8 shows the predicted RV amplitude as a function of orbital period for four groups of planets: Plot A includes the full catalog of planets, Plot B includes all planets with radii $\leq 2 R_{\oplus}$, Plot C includes the $> 0\%$ HZ planets and Plot D includes $> 0\%$ HZ planets with radii $\leq 2R_{\oplus}$. For planets that were missing mass measurements for the RV amplitude calculations, predicted values from Chen & Kipping (2018) were used. These planets are denoted by an *X* symbol, and observations of these planets to obtain mass measurements is paramount. Planets represented with a dot have mass measurements, but many would benefit from RV followup to refine their orbit and mass measurements.

The plots are color-coded by *V* magnitude (*V*), as indicated by the color-bar on the right. A magnitude cutoff of $V = 14$ mag was applied as this is pushing the limit of the best ground-based RV telescopes today. This limit removed the majority of the $> 0\%$ HZ planets with radii $\leq 2R_{\oplus}$ (Plot D).

Current state-of-the-art extreme precision radial velocity (EPRV) instruments such as NEID (Halverson et al. 2016), ESPRESSO (Pepe et al. 2021), and EXPRES (Petersburg et al. 2020) are capable of achieving sub 30 cm/s single measurement precision (SMP) and around 50 cm/s long-term precision over several months for nearby bright stars (Pepe et al. 2021). Such instruments would significantly improve the mass measurements for planets around nearby stars that already have mass values measured thanks to their improved RV precisions over their predecessors, which typically is on the order of a few m/s. Spectrograph performance, however, is highly dependent on the signal-to-noise ratio (SNR) of each measurement and RV measurement precision generally decreases for fainter stars because of the difficulty of achieving high enough SNR (Fischer et al. 2016). Obtaining robust mass measurements for HZ terrestrial planets around faint stars that induce RV

semi-amplitudes of only < 50 cm/s may still be out of the current capabilities even with the latest EPRV spectrographs.

In order to increase the number of planets in this group, investment into ground-based large aperture telescopes and EPRV instruments are paramount to the complete characterization of habitable zone terrestrial planets and their atmospheres.

4.6. *Additional Notes*

Only the default values were downloaded from the NEA for each planet included in this paper. The NEA designates a single paper per planet from which it extracts the default planet and star parameters. Because of this, there are instances where the default parameters for a planet is taken from a paper that does not provide measurements for all parameters, even though there are other papers that have measured the parameter (i.e. a RV paper that does not state the radius measured in a previous transit survey). As mixing parameters from different studies can lead to errors due to inconsistent methodology, we elected to only use the default parameters and calculate missing parameters where possible. We recommend the reader investigate all papers listed on the NEA for any particular planet of interest to determine the best parameters available.

5. CONCLUSIONS

In this paper, we present a complete catalog (at time of writing) of planets that orbit within or through the HZ, including the HZ boundaries and the percentage of the orbital period that each planet spends in their star’s HZ. Observational metrics for each planet, such as TSM values and RV amplitude, are included to facilitate selection for future follow-up observations.

Demographics of Rocky-OHZ, 100%HZ, $> 0\%$ HZ, and the full catalog of exoplanets are explored in Section 4, and various planets are highlighted as potential targets to test the boundaries of habitability.

Histograms of Rocky-OHZ, 100%HZ, $> 0\%$ HZ, and the full catalog of exoplanets are discussed in Section 4. There is a lack of planets in the sub-Saturn radius valley for the 100%HZ, $> 0\%$ HZ, and the full catalog of exoplanets. Observational biases may be driving this gap but as the gap is seen amongst the HZ planets, where the RV signature of a $\geq 10 M_{\oplus}$ is well within the capability of detection by current technology for most stars, we believe further investigation into whether this gap is real is warranted.

The small planet radius gap may be evident in each of the 100%HZ, $> 0\%$ HZ, and full catalog groups of planets. Due to small number statistics driven by the

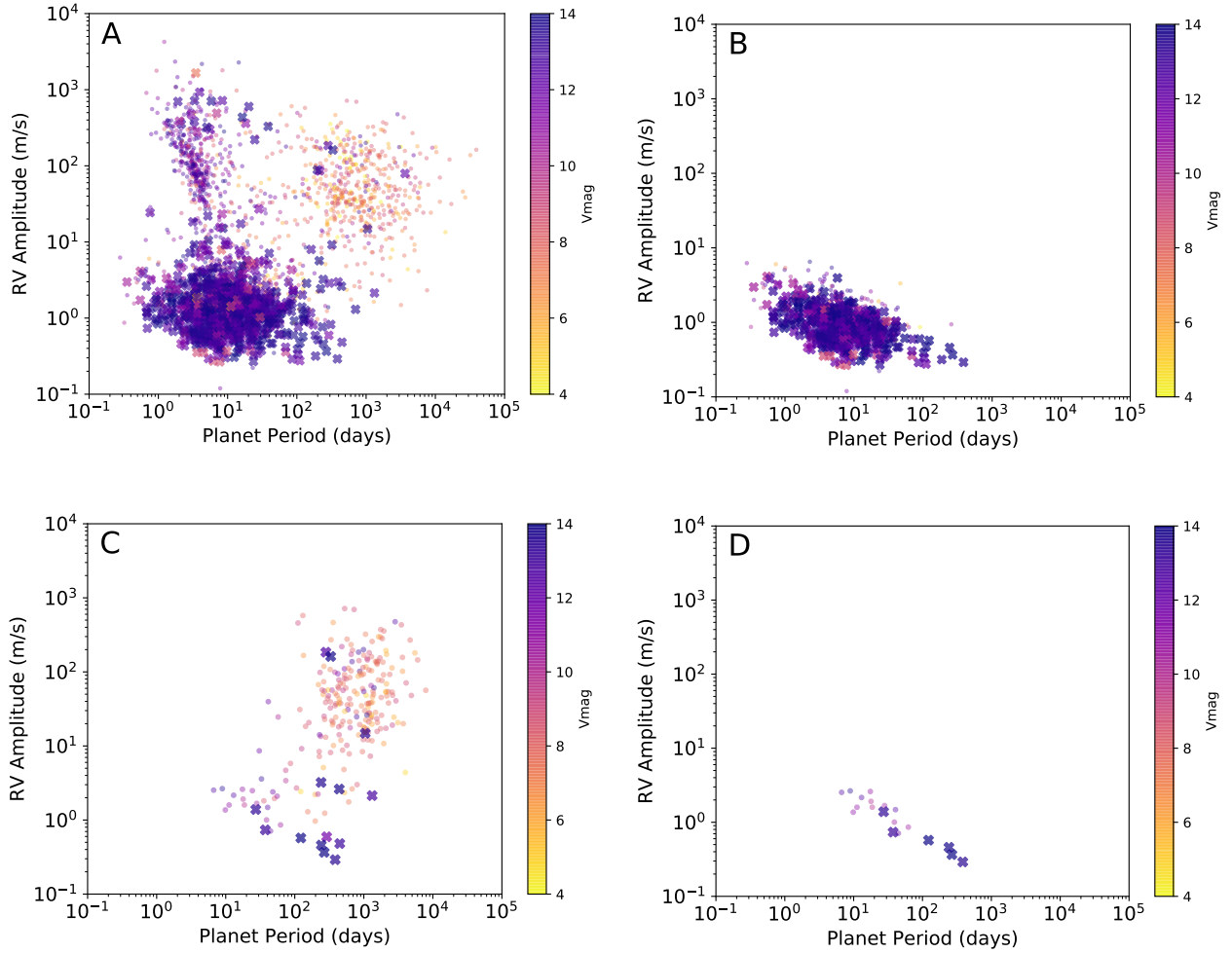


Figure 8. Predicted RV amplitude as a function of orbital period for four groups of planets: Plot A includes the full catalog of planets, Plot B includes all planets with radii $\leq 2R_{\oplus}$, Plot C includes the $> 0\%$ HZ planets and Plot D includes $> 0\%$ HZ planets with radii $\leq 2R_{\oplus}$. Planets that are missing mass measurements are denoted by an X symbol. Planets represented with a dot have mass measurements, but many would benefit from RV followup to refine their orbit and mass measurements. The plots are color-coded by V magnitude, as indicated by the color-bar on the right, with a V cutoff of 14 mag.

difficulty in finding low mass planets in the HZ we are unable to conclude whether this gap is real or due to observational biases. If the gap does exist, determining whether this gap amongst the HZ planets is caused by photoevaporation, core-powered mass-loss or some combination of the two will provide insight into the early atmospheric evolution of these HZ worlds. Each atmosphere loss mechanism has different implications for the atmospheric evolution and surface conditions of a planet, particularly of terrestrial HZ planets. Determining the existence and cause of this gap within the HZ planets is paramount.

Rocky-OHZ planets have predominantly low eccentricities. In general, longer period and larger mass planets tend to have a wider range of eccentricities than the shorter period planets.

TSM values for HZ planets are relatively low compared with the full inventory of known exoplanets, mostly due to the low T_{eq} of these HZ planets. Of all the planets ($\leq 10 R_{\oplus}$) passing through and orbiting within the HZ, HD 102365 b and 55 Cnc f have the greatest TSM values. The $\leq 2 R_{\oplus}$ HZ planets with the highest TSM values include GJ 667 C c, Teegarden’s Star b, Wolf 1061 c and Proxima Cen b.

Observational biases drive many of the features seen in the demographics. Transit surveys are optimised to discover planets around smaller, fainter stars and RV surveys are optimised for brighter, sun-like stars. This causes a bi-modal distribution and a possibly misleading valley to appear in the histograms of both J and T_{eff} . In the planet period versus planet mass plot of Figure 5, the plot suggests that larger stars tend to host

more massive planets in the HZ, however this is likely influenced by the increased difficulty in trying to detect lower mass planets around larger stars. The lack of HZ planets detected around highly evolved stars, as seen in Figure 6, is again likely due to an observational bias. Detecting HZ planets around these massive stars may be beyond current capabilities, as the transit depth of existing planets reduces as these stars expand, and RV surveys tend to focus on the more stable main sequence stars.

The inventory of HZ planets will continue to increase as current exoplanet surveys, such as TESS (Ricker et al. 2015) and CHEOPS (Broeg et al. 2014), provide new discoveries and characterization opportunities. With the recommendations of the Decadal Survey on Astronomy and Astrophysics 2020 focusing on the detection and characterisation of habitable exoplanets (of Sciences Engineering & Medicine 2021b), observations of known HZ planets from this catalog, particularly of the more extreme planets such as those described in Section 4.2, are vital. These observations will help determine if the HZ is a useful tool and will facilitate testing of the boundaries of habitability. These more extreme planets are important targets for future observations as they will provide insight into the habitability of planets with high eccentricity, high or low density, circumbinary planets or those orbiting evolved stars along with positioning in and around the HZ. It is essential to follow-up many of these edge case planets to thoroughly test the boundaries of habitability and the robustness of planetary atmospheric evolution. The JWST is set to observe some of the highest measured density HZ planets, such as the TRAPPIST-1 system (Lustig-Yaeger et al. 2019). Detection and characterisation of any atmospheres on TRAPPIST-1 d,e,f, and g will provide useful insight into the habitability of planets around M-dwarf stars, as well as allow comparative planetology of multiple planets within the HZ. As a similar historical stellar environment can be assumed for each planet, this direct comparison of terrestrial planets at varying distances within

the HZ is ideal for determining how habitability changes with position within the HZ.

The list of known exoplanets continues to grow, with over 5000 confirmed planets and many more awaiting confirmation. While large pools of planets are particularly good for statistical and demographic studies, it presents a significant target selection challenge in the search for potentially habitable planets in quantifying which may be most suitable from both an astrobiological and observation perspective. This is where target selection tools such as the HZ are most useful. By refining the full catalog of planets to only those whose orbits lie within an area around the star where conditions are most conducive to the existence of liquid water on the surface, limited telescope time can be directed to the most promising targets. Observations of the planets in this catalog with JWST and future missions, such as the Nancy Grace Roman Space Telescope (Kasdin et al. 2020), LUVOIR (The LUVOIR Team 2019) and HabEx (Gaudi et al. 2020), will provide further insight into the habitability of exoplanets found in the HZ. By using this catalog and the planets highlighted within it to guide target selection, the boundaries of habitability can be investigated and the reliability of the HZ hypothesis assessed.

ACKNOWLEDGEMENTS

M.H. would like to acknowledge NASA support via the FINESST Planetary Science Division, NASA award number 80NSSC21K1536. M.H. Would also like to thank Hilke Schlichting for her advice regarding the radius valley of HZ planets. T.F. acknowledges support from the University of California President’s Postdoctoral Fellowship Program. This research has made use of the NASA Exoplanet Archive. We obtain the data set from the NASA Exoplanet Archive (NASA Exoplanet Archive 2022)¹ This dataset or service is made available by the NASA Exoplanet Science Institute at IPAC, which is operated by the California Institute of Technology under contract with the National Aeronautics and Space Administration. This research has also made use of the Habitable Zone Gallery at hzgallery.org.

REFERENCES

- Abe, Y., Abe-Ouchi, A., Sleep, N. H., & Zahnle, K. J. 2011, *Astrobiology*, 11, 443
- Adams, A. D., & Kane, S. R. 2016, *AJ*, 152, 4
- Akeson, R. L., Chen, X., Ciardi, D., et al. 2013, *PASP*, 125, 989
- Anglada-Escudé, G., Tuomi, M., Gerlach, E., et al. 2013, *A&A*, 556, A126
- Anglada-Escudé, G., Amado, P. J., Barnes, J., et al. 2016, *Nature*, 536, 437

¹ Accessed on 2022-05-19 at 12:45, returning 4550 rows.

- Batalha, N. M., Borucki, W. J., Koch, D. G., et al. 2010, *The Astrophysical Journal*, 713, L109
- Belu, A. R., Selsis, F., Raymond, S. N., et al. 2013, *ApJ*, 768, 125
- Bennett, D. P., Ranc, C., & Fernandes, R. B. 2021, *The Astronomical Journal*, 162, 243
- Berger, T. A., Huber, D., van Saders, J. L., et al. 2020, *AJ*, 159, 280
- Bonfils, X., Delfosse, X., Udry, S., et al. 2013, *A&A*, 549, A109
- Borucki, W. J. 2016, *Reports on Progress in Physics*, 79, 036901
- Bowler, B. P., Liu, M. C., Shkolnik, E. L., & Tamura, M. 2015, *ApJS*, 216, 7
- Broeg, C., Benz, W., Thomas, N., & Cheops Team. 2014, *Contributions of the Astronomical Observatory Skalnaté Pleso*, 43, 498
- Bryson, S., Kunimoto, M., Kopparapu, R. K., et al. 2021, *AJ*, 161, 36
- Burke, C. J., Mullally, F., Thompson, S. E., Coughlin, J. L., & Rowe, J. F. 2019, *AJ*, 157, 143
- Chandler, C. O., McDonald, I., & Kane, S. R. 2016, *AJ*, 151, 59
- Chen, J., & Kipping, D. 2017, *ApJ*, 834, 17
- Chen, J., & Kipping, D. M. 2018, *MNRAS*, 473, 2753
- Collins, K. A., Eastman, J. D., Beatty, T. G., et al. 2014, *AJ*, 147, 39
- Cukier, W., Kopparapu, R. k., Kane, S. R., et al. 2019, *PASP*, 131, 124402
- Cuntz, M. 2014, *ApJ*, 780, 14
- Dalal, S., Kiefer, F., Hébrard, G., et al. 2021, *A&A*, 651, A11
- Dalba, P. A., Fulton, B., Isaacson, H., Kane, S. R., & Howard, A. W. 2020, *AJ*, 160, 149
- Dedrick, C. M., Fulton, B. J., Knutson, H. A., et al. 2021, *AJ*, 161, 86
- Díaz, R. F., Ségransan, D., Udry, S., et al. 2016a, *A&A*, 585, A134
- Díaz, R. F., Rey, J., Demangeon, O., et al. 2016b, *A&A*, 591, A146
- Dong, C., Lingam, M., Ma, Y., & Cohen, O. 2017, *ApJL*, 837, L26
- Doyle, L. R., Carter, J. A., Fabrycky, D. C., et al. 2011, *Science*, 333, 1602
- Dreizler, S., Jeffers, S. V., Rodríguez, E., et al. 2020, *MNRAS*, 493, 536
- Dressing, C. D., & Charbonneau, D. 2013, *ApJ*, 767, 95
- . 2015, *ApJ*, 807, 45
- Emsenhuber, A., Mordasini, C., Burn, R., et al. 2021, *A&A*, 656, A69
- Fischer, D. A., Marcy, G. W., Butler, R. P., et al. 2001, *ApJ*, 551, 1107
- . 2008, *ApJ*, 675, 790
- Fischer, D. A., Anglada-Escude, G., Arriagada, P., et al. 2016, *PASP*, 128, 066001
- Ford, E. B. 2014, *Proceedings of the National Academy of Science*, 111, 12616
- Fujii, Y., Angerhausen, D., Deitrick, R., et al. 2018, *Astrobiology*, 18, 739
- Fulton, B. J., Petigura, E. A., Howard, A. W., et al. 2017, *AJ*, 154, 109
- Gaidos, E. 2013, *ApJ*, 770, 90
- Gaudi, B. S., Seager, S., Mennesson, B., et al. 2020, arXiv e-prints, arXiv:2001.06683
- Gillon, M., Jehin, E., Lederer, S. M., et al. 2016, *Nature*, 533, 221
- Ginzburg, S., Schlichting, H. E., & Sari, R. 2018, *Monthly Notices of the Royal Astronomical Society*, 476, 759
- Glaser, D. M., Hartnett, H. E., Desch, S. J., et al. 2020, *ApJ*, 893, 163
- Gupta, A., & Schlichting, H. E. 2019, *Monthly Notices of the Royal Astronomical Society*, 487, 24
- Haghighipour, N., & Kaltenegger, L. 2013, *ApJ*, 777, 166
- Haghighipour, N., Vogt, S. S., Butler, R. P., et al. 2010, *ApJ*, 715, 271
- Halverson, S., Terrien, R., Mahadevan, S., et al. 2016, in *Society of Photo-Optical Instrumentation Engineers (SPIE) Conference Series*, Vol. 9908, Ground-based and Airborne Instrumentation for Astronomy VI, ed. C. J. Evans, L. Simard, & H. Takami, 99086P
- Hayashi, C. 1981, *Progress of Theoretical Physics Supplement*, 70, 35
- Heller, R. 2012, *A&A*, 545, L8
- Heller, R., & Armstrong, J. 2014, *Astrobiology*, 14, 50
- Heller, R., & Barnes, R. 2013, *Astrobiology*, 13, 18
- Hill, M. L., Kane, S. R., Seperuelo Duarte, E., et al. 2018, *ApJ*, 860, 67
- Hsu, D. C., Ford, E. B., Ragozzine, D., & Ashby, K. 2019, *The Astronomical Journal*, 158, 109
- Ida, S., & Lin, D. N. C. 2004, *ApJ*, 604, 388
- Jenkins, J. M., Twicken, J. D., Batalha, N. M., et al. 2015, *AJ*, 150, 56
- Johnson, J. A., Clanton, C., Howard, A. W., et al. 2011, *ApJS*, 197, 26
- Jones, H. R. A., Butler, R. P., Tinney, C. G., et al. 2006, *MNRAS*, 369, 249
- Kane, S. R. 2014, *ApJ*, 782, 111
- . 2018, *ApJL*, 861, L21
- Kane, S. R., Ciardi, D. R., Gelino, D. M., & von Braun, K. 2012, *MNRAS*, 425, 757

- Kane, S. R., & Gelino, D. M. 2012a, *Astrobiology*, 12, 940
 —. 2012b, *PASP*, 124, 323
- Kane, S. R., Henry, G. W., Dragomir, D., et al. 2011a, *ApJL*, 735, L41
- Kane, S. R., & Hinkel, N. R. 2013, *ApJ*, 762, 7
- Kane, S. R., Kopparapu, R. K., & Domagal-Goldman, S. D. 2014, *ApJL*, 794, L5
- Kane, S. R., Li, Z., Wolf, E. T., Ostberg, C., & Hill, M. L. 2021, *AJ*, 161, 31
- Kane, S. R., Mahadevan, S., von Braun, K., Laughlin, G., & Ciardi, D. R. 2009, *PASP*, 121, 1386
- Kane, S. R., Turnbull, M. C., Fulton, B. J., et al. 2020, *AJ*, 160, 81
- Kane, S. R., Howard, A. W., Pilyavsky, G., et al. 2011b, *ApJ*, 733, 28
- Kane, S. R., Dragomir, D., Ciardi, D. R., et al. 2011c, *ApJ*, 737, 58
- Kane, S. R., Hill, M. L., Kasting, J. F., et al. 2016, *ApJ*, 830, 1
- Kasdin, N. J., Bailey, V. P., Mennesson, B., et al. 2020, in *Space Telescopes and Instrumentation 2020: Optical, Infrared, and Millimeter Wave*, ed. M. Lystrup, M. D. Perrin, N. Batalha, N. Siegler, & E. C. Tong, Vol. 11443, International Society for Optics and Photonics (SPIE), 300 – 313
- Kasting, J. F., Whitmire, D. P., & Reynolds, R. T. 1993, *Icarus*, 101, 108
- Kempton, E. M. R., Bean, J. L., Louie, D. R., et al. 2018, *PASP*, 130, 114401
- Kipping, D., Bryson, S., Burke, C., et al. 2022, *Nature Astronomy*, arXiv:2201.04643
- Kopparapu, R. K., & Barnes, R. 2010, *ApJ*, 716, 1336
- Kopparapu, R. K., Ramirez, R. M., SchottelKotte, J., et al. 2014, *ApJ*, 787, L29
- Kopparapu, R. K., Ramirez, R., Kasting, J. F., et al. 2013, *ApJ*, 765, 131
- Kopparapu, R. K., Hébrard, E., Belikov, R., et al. 2018, *ApJ*, 856, 122
- Kostov, V. B., Orosz, J. A., Welsh, W. F., et al. 2016, *ApJ*, 827, 86
- Kunimoto, M., & Matthews, J. M. 2020, *The Astronomical Journal*, 159, 248
- Lambrechts, M., & Johansen, A. 2014, *Astronomy & Astrophysics*, 572, doi:10.1051/0004-6361/201424343
- Lammer, H., Selsis, F., Ribas, I., et al. 2003, *The Astrophysical Journal*, 598, L121
- Lisse, C. M., Desch, S. J., Unterborn, C. T., et al. 2020, *ApJL*, 898, L17
- Lopez, E. D., & Fortney, J. J. 2013, *ApJ*, 776, 2
- Lustig-Yaeger, J., Meadows, V. S., & Lincowski, A. P. 2019, *AJ*, 158, 27
- Martin, D. V., & Triaud, A. H. M. J. 2015, *MNRAS*, 449, 781
- Mason, P. A., Zuluaga, J. I., Cuartas-Restrepo, P. A., & Clark, J. M. 2015, *International Journal of Astrobiology*, 14, 391
- Mayor, M., Marmier, M., Lovis, C., et al. 2011, arXiv e-prints, arXiv:1109.2497
- Montet, B. T., Crepp, J. R., Johnson, J. A., Howard, A. W., & Marcy, G. W. 2014, *ApJ*, 781, 28
- Morbidelli, A., Lambrechts, M., Jacobson, S., & Bitsch, B. 2015, *Icarus*, 258, 418
- Muirhead, P. S., Hamren, K., Schlawin, E., et al. 2012, *ApJL*, 750, L37
- Mullally, F., Thompson, S. E., Coughlin, J. L., Burke, C. J., & Rowe, J. F. 2018, *AJ*, 155, 210
- Müller, T. W. A., & Haghighipour, N. 2014, *ApJ*, 782, 26
- Murray-Clay, R. A., Chiang, E. I., & Murray, N. 2009, *The Astrophysical Journal*, 693, 23
- NASA Exoplanet Archive. 2022, *Planetary Systems*, v.Version: 2022-05-19 12:45, NExSci-Caltech/IPAC, doi:10.26133/NEA12
- of Sciences Engineering, N. A., & Medicine. 2021a, *Pathways to Discovery in Astronomy and Astrophysics for the 2020s* (Washington, DC: The National Academies Press), doi:10.17226/26141
- . 2021b, *Pathways to Discovery in Astronomy and Astrophysics for the 2020s*, doi:10.17226/26141
- Orosz, J. A., Welsh, W. F., Carter, J. A., et al. 2012, *Science*, 337, 1511
- Orosz, J. A., Welsh, W. F., Haghighipour, N., et al. 2019, *AJ*, 157, 174
- Owen, J. E., & Wu, Y. 2013, *ApJ*, 775, 105
- Palubski, I., Shields, A., & Deitrick, R. 2020, arXiv e-prints, arXiv:2001.02228
- Pepe, F., Cristiani, S., Rebolo, R., et al. 2021, *A&A*, 645, A96
- Petersburg, R. R., Ong, J. M. J., Zhao, L. L., et al. 2020, *AJ*, 159, 187
- Pilyavsky, G., Mahadevan, S., Kane, S. R., et al. 2011, *ApJ*, 743, 162
- Popp, M., & Eggl, S. 2017, *Nature Communications*, 8, 14957
- Quintana, E. V., Barclay, T., Raymond, S. N., et al. 2014, *Science*, 344, 277
- Ramirez, R. M., & Kaltenegger, L. 2018, *ApJ*, 858, 72
- Ricker, G. R., Winn, J. N., Vanderspek, R., et al. 2015, *Journal of Astronomical Telescopes, Instruments, and Systems*, 1, 014003

- Robertson, P., & Mahadevan, S. 2014, *ApJL*, 793, L24
- Rogers, J. G., Gupta, A., Owen, J. E., & Schlichting, H. E. 2021, *Monthly Notices of the Royal Astronomical Society*, 508, 5886
- Rowe, J. F., Bryson, S. T., Marcy, G. W., et al. 2014, *ApJ*, 784, 45
- Schwieterman, E. W., Reinhard, C. T., Olson, S. L., Harman, C. E., & Lyons, T. W. 2019, *The Astrophysical Journal*, 878, 19
- Schwieterman, E. W., Kiang, N. Y., Parenteau, M. N., et al. 2018, *Astrobiology*, 18, 663
- Socia, Q. J., Welsh, W. F., Orosz, J. A., et al. 2020, *AJ*, 159, 94
- Suzuki, D., Bennett, D. P., Ida, S., et al. 2018, *The Astrophysical Journal*, 869, L34
- Teachey, A., Kipping, D. M., & Schmitt, A. R. 2017, *The Astronomical Journal*, 155, 36
- The LUVVOIR Team. 2019, arXiv e-prints, arXiv:1912.06219
- Thorngren, D. P., Marley, M. S., & Fortney, J. J. 2019, *Research Notes of the American Astronomical Society*, 3, 128
- Tinney, C. G., Butler, R. P., Jones, H. R. A., et al. 2011, *ApJ*, 727, 103
- Tuomi, M., Anglada-Escudé, G., Gerlach, E., et al. 2013, *A&A*, 549, A48
- Unterborn, C. T., Desch, S. J., Hinkel, N. R., & Lorenzo, A. 2018, *Nature Astronomy*, 2, 297
- Van-Eylen, V., & Albrecht, S. 2015, *The Astrophysical Journal*, 808, 126
- Vanderburg, A., Plavchan, P., Johnson, J. A., et al. 2016, *Monthly Notices of the Royal Astronomical Society*, 459, 3565
- Wang, J., Fischer, D. A., Barclay, T., et al. 2015, *ApJ*, 815, 127
- Way, M. J., Del Genio, A. D., Kiang, N. Y., et al. 2016, *Geophys. Res. Lett.*, 43, 8376
- Way, M. J., & Georgakarakos, N. 2017, *ApJ*, 835, L1
- Weiss, L. M., & Marcy, G. W. 2014, *ApJL*, 783, L6
- Weiss, L. M., Marcy, G. W., Petigura, E. A., et al. 2018, *AJ*, 155, 48
- Welsh, W. F., Orosz, J. A., Short, D. R., et al. 2015, *ApJ*, 809, 26
- Williams, D. M., & Pollard, D. 2002, *International Journal of Astrobiology*, 1, 61
- Winn, J. N., & Fabrycky, D. C. 2015, *ARA&A*, 53, 409
- Wittenmyer, R. A., Tinney, C. G., O’Toole, S. J., et al. 2011, *ApJ*, 727, 102
- Wolf, E. T., Haqq-Misra, J., Kopparapu, R., et al. 2020, *Journal of Geophysical Research (Planets)*, 125, e06576
- Wolfgang, A., Rogers, L. A., & Ford, E. B. 2016, *The Astrophysical Journal*, 825, 19
- Wright, D. J., Wittenmyer, R. A., Tinney, C. G., Bentley, J. S., & Zhao, J. 2016, *ApJL*, 817, L20
- Yang, J., Boué, G., Fabrycky, D. C., & Abbot, D. S. 2014, *ApJL*, 787, L2
- Zechmeister, M., Dreizler, S., Ribas, I., et al. 2019, *A&A*, 627, A49